Quantum Spin Liquid Ground States of the Heisenberg-Kitaev Model on the Triangular Lattice

Pavel Kos

Elite Master Program
Theoretical and Mathematical Physics
Ludwig–Maximilians–Universität München

A thesis submitted for the degree of
Master of Science

Supervisor: Prof. Dr. Matthias Punk

München 2016

Abstract

In this master thesis, we investigate quantum disordered spin liquid ground states of the Heisenberg-Kitaev model on the triangular lattice using Schwinger-boson mean-field theory. Our goal is to identify and characterize potential gapped spin liquid ground states. After reviewing known results of Heisenberg-Kitaev model, projective symmetry group (PSG) analysis is carried out to determine the possible mean-field ansatzes.

We focus on the only totally symmetric ansatz and compute the mean-field parameters self-consistently. Depending on the ratio of Kitaev and Heisenberg coupling, we find three spin liquid ground states separated by two continuous phase transitions. To characterise these phases, we compute one spinon dispersions, static spin structure factors and examine their classical limits. Close to the Heisenberg point we find SU(2) invariant zero-flux phase known from studies of the Heisenberg model on the triangular lattice. In the opposite Kitaev-limit, a spin liquid that has the classical ground state of the Kitaev model as its classical limit is found. Interestingly, at intermediate couplings we observe a novel spin liquid ground state with non-zero couplings of different spin components.

Acknowledgements

I would first like to thank my supervisor Matthias Punk for guidance, discussions and for answering my questions.

I am grateful to Jad C. Halimeh for interesting discussions connected to my thesis and for reading my thesis.

Furthermore I want to thank Martin Dupont for improving the English of this thesis.

I enyojed my studies at TMP, so I would like to thank students and Robert Helling for two very interesting years of my life.

I want to thank Tina, for motivating me and listening to my ramblings.

I would also like to thank my parents Marjanca and Ivan and sister Anja for always being curious about the world and infecting me with the curiosity.

Last but not least I want to acknowledge Slovene human resources development and scholarship fund (Javni sklad Republike Slovenije za razvoj kadrov in štipendije) for supporting my studies with Ad futura scholarship (No. 11010-234/2014).

The universal wave function and its boundary conditions are also acknowledged.

Contents

Chapter 1

Introduction

Quantum spin models are a very important and popular class of systems describing insulating materials with localized magnetic moments. Not only are they relevant for many materials, they are intrinsically quantum mechanical and show many non classical counterintuitive phenomena. Having a finite number of degrees of freedom per lattice site, they are one of the simplest quantum many-body systems. This makes them prototypical examples for studying quantum many-body phenomena such as thermal and quantum phase transitions, as well as non-equilibrium phenomena.

Furthermore, the relative simplicity of spin systems in one and two dimensions leads to some exact solutions that are fundamentally important and can also be a check for numerical methods.

There are many new concepts which were developed and used in the study of spin systems. From the Bethe ansatz methods and the Jordan-Wigner transformation in one dimensional systems to the semiclassical spin wave theory in ordered systems, the renormalization group studies and many others.

In the past decades, there was a lot of interest in new topological phases of matter called spin liquid phases. They do not exhibit magnetic order down to zero temperature [1] and have no direct classical analogs. The spin liquid ground states are expected to occur in frustrated systems, which lack an obvious way of ordering.

Treatment of these phases naturally leads to emergent gauge fields and lattice quantum field theory [2]. We encounter the famous confinement problem from QCD. Studying the degeneracy of ground states on the torus or excitations, the topological nature of the phase is seen. It is also interesting to look at spin liquids from the viewpoint of entanglement and entanglement entropy [3]. The topological nature has lead to a lot of interest in quantum information, hinting at the solution of the quantum decoherence problem.

Combining the symmetries and topological nature of the phase, we encounter new exotic symmetry enriched topological (SET) phases. They can be partially classified using projective symmetry group (PSG) [4].

Evidently, studying spin systems combines a lot of exciting new theoretical concepts from many branches of physics. Hence we decided to study a specific geometrically and chemically frustrated model in this thesis.

This so-called Kitaev-Heisenberg model on the triangular lattice arises naturally as an effective model of Iridium Mott insulators [5, 6]. The geometrical frustration of the model is a consequence of the triangular lattice. Moreover, strong spin-orbit coupling gives rise to direction-dependent Kitaev couplings, chemically frustrating

the system. Previous works have shown that the model can exhibit interesting magnetically ordered states, for example the $\mathbb{Z}_2$ vortex crystal [7, 6]. Our approach is to look for quantum disordered spin liquid ground states using Schwinger-boson mean-field theory (SBMFT). Even though SBMFT does not give quantitatively accurate results, it is a very useful tool to construct and characterize potential spin liquid states and to analyze their qualitative behavior [8, 9]. Furthermore, it allows us to make connections to earlier work on magnetically ordered states by studying the semi-classical large spin S limit.

Furthermore, we used the projective symmetry group (PSG) approach to determine possible ansatzes. Later on, we focused on the only totally symmetric ansatz, determined the parameters self-consistently and characterised resulting phases by dispersion, static spin structure factor and their classical limit.

Chapter 2

Theoretical Background

Spin systems are a very interesting playground of theoretical physics and are also highly relevant for real materials. They arise naturally from Mott insulators. Furthermore, quantum spin systems are one of the most important examples of strongly correlated many body systems.

The prime examples of quantum spin models are given by the Heisenberg Hamiltonian:

$$H_H = \frac{1}{2} \sum_{\substack{i,j \\ i \neq j}} J_{ij} \mathbf{S_i} \cdot \mathbf{S_j}, \tag{2.1}$$

where $\mathbf{S_i}$ and $\mathbf{S_j}$ are spin operators acting on i and j lattice sites. J_{ij} is the exchange coupling constant coupling these two sites. Usually the interactions are taken to be short range, e. g. nearest neighbours interactions and site-independent:

$$H_H = J \sum_{\langle i,j \rangle} \mathbf{S_i} \cdot \mathbf{S_j}, \tag{2.2}$$

where $\langle i, j \rangle$ denotes the sum over nearest neighbours.

Depending on the sign of J and the geometry of the lattice, the ground states can exhibit well known ordered ferromagnetic (J<0) and antiferromagnetic (J>0) phases, as shown in Figure 2.1. In the cases where the system is frustrated, the ground state can be a novel quantum spin liquid (QSL) phase.

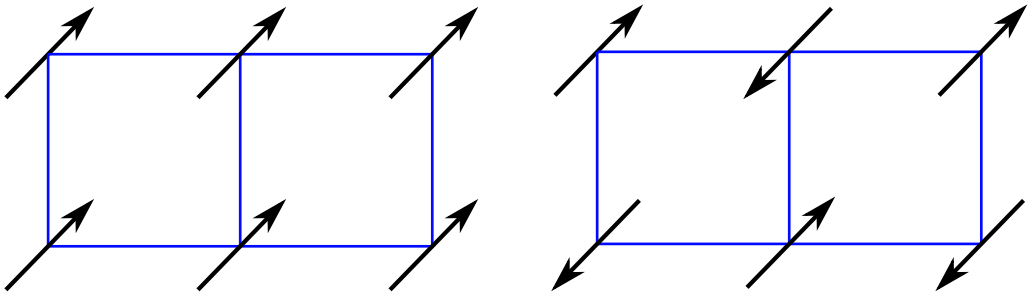

Figure 2.1: Ferromagnetic order shown on the left and antiferromagnetic order on the right.

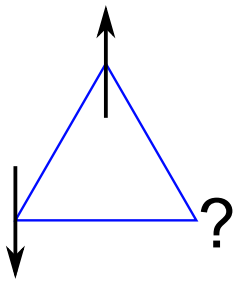

Figure 2.2: Triangle of antiferromagnetically interacting Ising spins illustrates the concept of frustration. All three spins can not be anti-parallel to each other. The ground state is 6-fold degenerate.

2.1 Quantum Spin Liquids

By lowering the temperature, the thermal fluctuations will become smaller and smaller. Normally this leads to an ordered ground state, but depending on the problem, because of low dimensionality and small spin (ideally S=1/2) we have strong quantum fluctuations. They can prevent magnetic long-range ordering even at zero temperature [1], resulting in a disordered quantum state called quantum spin liquid (QSL). We can view quantum fluctuations as a consequence of the uncertainty principle.

In cases where the classical ground state is highly degenerate, the quantum fluctuations become more apparent and the likelihood of having a QSL ground state is increased. We say that the system is frustrated. A simple example of geometric frustration is shown in Figure 2.2. Geometric frustration is usually a consequence of antiferromagnetic exchange interactions in combination with the geometry of the lattice, the most famous examples are the two-dimensional kagome and triangular lattices and the three-dimensional pyrochlore lattice. A similar way to achieve frustration is to have competing incompatible interactions, for example antiferromagnetic nearest neighbour couplings and next neighbour couplings on a square lattice.

The main features of QSLs are [3]: anomalously high degree of entanglement (massive superposition) and non-local excitations (e.g spinons - quasiparticles with spin 1/2 and no electric charge). Two-dimensional systems are especially interesting, because they can exhibit anyonic excitations, meaning that the the exchange of two particles gives a phase that is neither 0 (bosons) nor π (fermions).

2.1.1 Describing Quantum Spin Liquids

1/S Expansion

Standard approach to describe antiferromagnetic phase is the semi-classical 1/S expansion. It uses the Holstein-Primakoff representation of the spin operators with bosons:

$$S_i^z = S - a_i a_i^\dagger, \tag{2.3a}$$

$$S^+ = \sqrt{2S - a_i^\dagger a_i}\, a_i, \tag{2.3b}$$

$$S^- = a_i^\dagger \sqrt{2S - a_i^\dagger a_i}. \tag{2.3c}$$

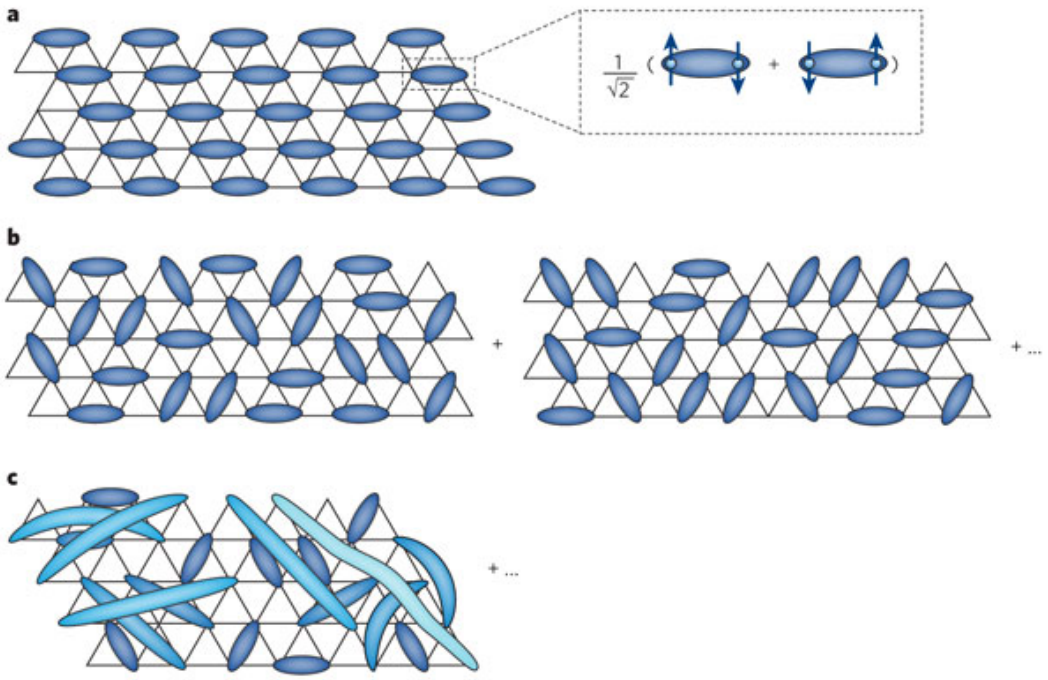

Figure 2.3: Valence-bond solid is a covering of the lattice by pairs of entangled spins. Resonating valence-bond state is a superposition of many different pairings. It can consist of short ranged (b) or long ranged (c) pairings. Taken from [1].

One can check that the spin operator algebra is preserved if we demand $[a_i, a_i^\dagger] = 1$. The idea is to start from a classical ground state configuration and assume that the quantum deviations are small $a_i^\dagger a_i \ll S$. Then one can expand the square root operator in a Taylor series of $1/S$.

But for quantum spin liquids this approach fails, since the expectation value of spin operator is 0 and we have $2S \approx \langle a_i^\dagger a_i \rangle$ [10]. So we need to find another way to describe QSLs. One possibility is to use Schwinger-Boson mean-field theory, which will be discussed in detail in Chapter 3.

Valence-Bond Picture

We try to look at the problem from the other limit. Let us examine wave functions built from singlets $|[ij]\rangle = \frac{1}{\sqrt{2}}(|\uparrow_i\downarrow_j\rangle - |\downarrow_i\uparrow_j\rangle)$.

$$|\mathrm{VB}\rangle = |[i_0 i_1] \otimes |[i_2 i_3]\rangle \otimes |[i_4 i_5]\rangle \otimes ... \tag{2.4}$$

Here, every lattice site appears exactly once. A pictorial representation is shown in Figure 2.3. There are some models where valence-bond (VB) wave function is an exact ground state or a good starting point, but they break some lattice symmetries. That is why these states are sometimes called valence-bond solids (VBS).

The resonating valence-bond (RVB) picture [11] is a way of obtaining spin liquid ground states out of valence-bond states. In RVB the ground state is a linear superposition of many different VB states. The superposition restores the symmetries and QSL state is formed. Because it consists of singlets we have perfect short range antiferromagnetic correlations but no long range antiferromagnetic order.

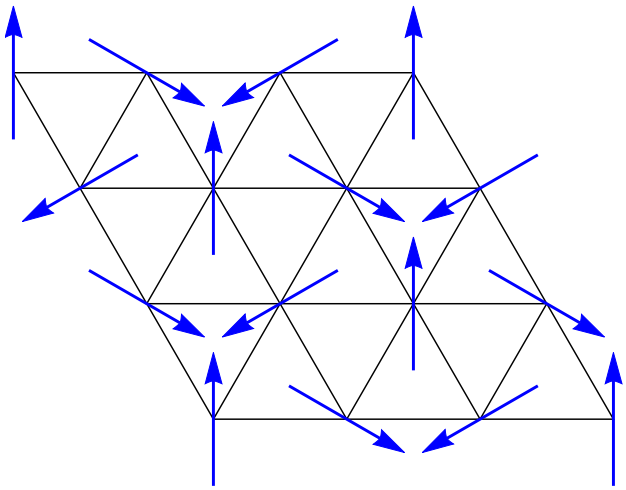

Figure 2.4: Ground state of nearest neighbour Heisenberg antiferromagnet on the triangular lattice: 120-degree order.

2.2 Heisenberg Model on the Triangular Lattice

The Heisenberg model on the triangular lattice has been the focus of numerous studies, using many different numerical and analytical techniques. The community has come to the consensus that the spin 1/2 antiferromagnetic nearest neighbour Heisenberg model on the triangular lattice exhibits a 120-degree coplanar order in the ground state [2]. It is shown in Figure 2.4.

2.3 Kitaev Model on the Hexagonal Lattice

Here we quickly mention the Kitaev model on the Hexagonal Lattice, introduced by Alexei Kitaev in 2006 [12]. Its interactions are anisotropic - two neighbours that lie in direction γ are coupled only by $S^\gamma S^\gamma$. Definition of links is shown in Figure 2.5.

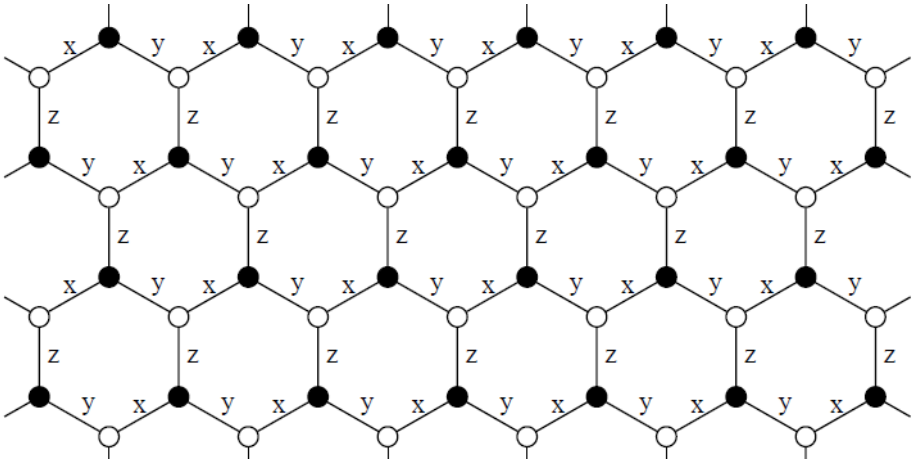

Figure 2.5: Honeycomb lattice and labeling of links in Kitaev model. Figure from Kitaev's paper [12].

Kitaev model is given by a following Hamiltonian:

$$H = -J_x \sum_{\text{x-links}} \sigma_i^x \sigma_j^x - J_y \sum_{\text{y-links}} \sigma_i^y \sigma_j^y - J_z \sum_{\text{z-links}} \sigma_i^z \sigma_j^z, \tag{2.5}$$

where σ^γ denote the Pauli matrices, and $S^\gamma = \frac{\sigma^\gamma}{2}$.

Remarkable property of this model is that it can be solved exactly. It has been shown that its ground state is a quantum spin liquid, has a nontrivial topological order and both abelian and non-abelian anyon quasiparticles are present in a magnetic field [13].

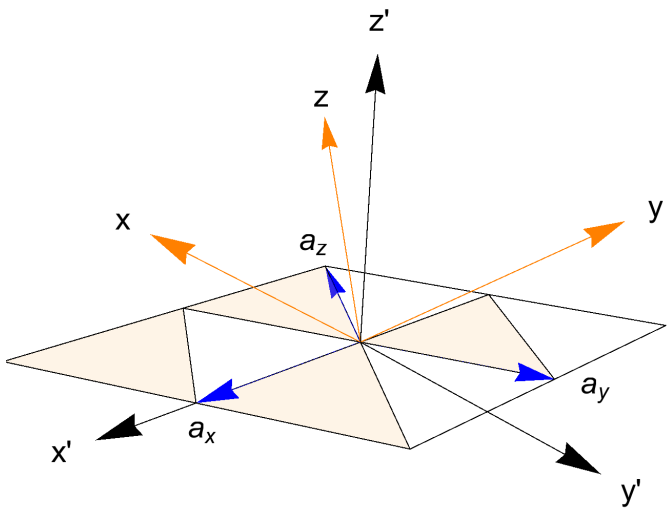

Figure 2.6: Definition of the triangular lattice vectors a_γ and the coordinate systems $\{x, y, z\}$ and $\{x', y', z'\}$. Operators S^γ act along the γ direction.

2.4 The Heisenberg-Kitaev Model on the Triangular Lattice

This thesis focuses on the study of the Heisenberg-Kitaev model on the triangular lattice, which has the following Hamiltonian:

$$H_{HK} = J_H \sum_{\langle ij \rangle} \mathbf{S_i} \cdot \mathbf{S_j} + J_K \sum_{\gamma || \langle ij \rangle} S_i^\gamma S_j^\gamma, \tag{2.6}$$

where $\mathbf{S_i}$ is a spin operator located on a triangular lattice site i and the sum runs over nearest-neighbor sites. The first term describes the usual isotropic Heisenberg interaction, whereas the second Kitaev interaction term explicitly breaks spin-rotation

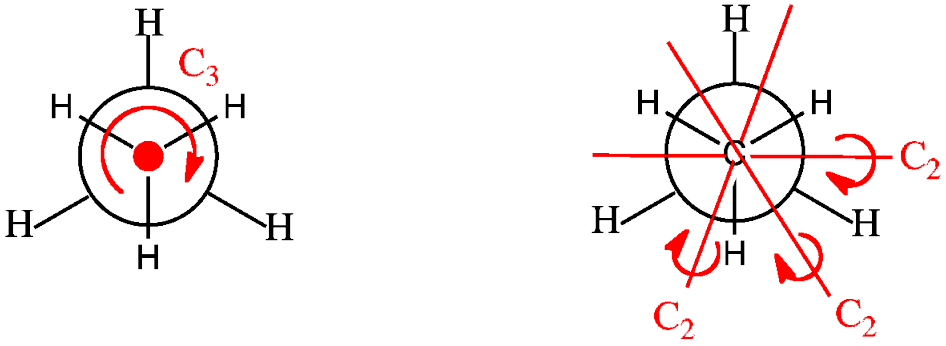

Figure 2.7: The most common example of D_{3d} symmetry group is the staggered ethane. On the left is shown the threefold rotation C_3, whereas on the right the three axes of twofold rotations C_2 are shown. Figure taken from www.chemtube3d.com.

invariance. It couples only the γ components S^γ of the spin operators connected by the link with direction $\mathbf{a}_\gamma$. We parametrize the interaction by an angle

$$J_H = J\cos\psi, \qquad J_K = J\sin\psi. \tag{2.7}$$

The energy scale will be fixed by $J = \sqrt{J_H^2 + J_K^2} = 1$. The triangular lattice is spanned by the basis vectors $\mathbf{a_x} = \mathbf{e'_x}$ and $\mathbf{a_y} = -\frac{1}{2}\mathbf{e'_x} + \frac{\sqrt{3}}{2}\mathbf{e'_y}$, where the lattice constant was set to unity. Additionally we define $\mathbf{a_z} = -\frac{1}{2}\mathbf{e'_x} - \frac{\sqrt{3}}{2}\mathbf{e'_y} = -\mathbf{a_x} - \mathbf{a_y}$. Here we expressed the vectors in a primed coordinate system, where $\mathbf{e'_x}$ and $\mathbf{e'_y}$ is a pair of orthogonal vectors in the lattice plane and $\mathbf{e'_z}$ is perpendicular to the lattice.

Spin-orbit coupling locks the primed coordinate system to the unprimed one, which defines the orientation of the spin operators with respect to the lattice, i.e.the component S^γ points in the γ direction, as is shown in Figure 2.6. This coordinate system is fixed by the condition $\mathbf{e'_z} = (1,1,1)/\sqrt{3}$ and that $\mathbf{e_x}$ projected onto the lattice plane points into the direction of $\mathbf{e'_x}$.

The combined spin-orbit symmetry is D_{3d} [7], which is depicted in Figure 2.7. The threefold rotation C_3 around the $(1,1,1)$ axis act as:

$$C_3 : (\mathbf{a_x}, \mathbf{a_y}, \mathbf{a_z}) \to (\mathbf{a_y}, \mathbf{a_z}, \mathbf{a_x}), \tag{2.8a}$$
$$C_3 : (S^x, S^y, S^z) \to (S^y, S^z, S^x), \tag{2.8b}$$

the three twofold rotations C_2 have axes perpendicular to bonds, and the three reflection planes lie parallel to the bonds. There are additional symmetries in spin space D_{2h} that map $(1,1,1)$ to the other three axes $(-1,1,1)$, $(1,-1,1)$ and $(1,1,-1)$ via three twofold rotations C_2, and the inversion generator is time reversal operator [7].

2.5 Main Results From the Literature

In this section we will summarize the main results from the literature on the Heisenberg-Kitaev model on the triangular lattice. Firstly, we will mention the connection to real materials. Later on we will discuss Klein duality, folowing by known numerical and analytical results.

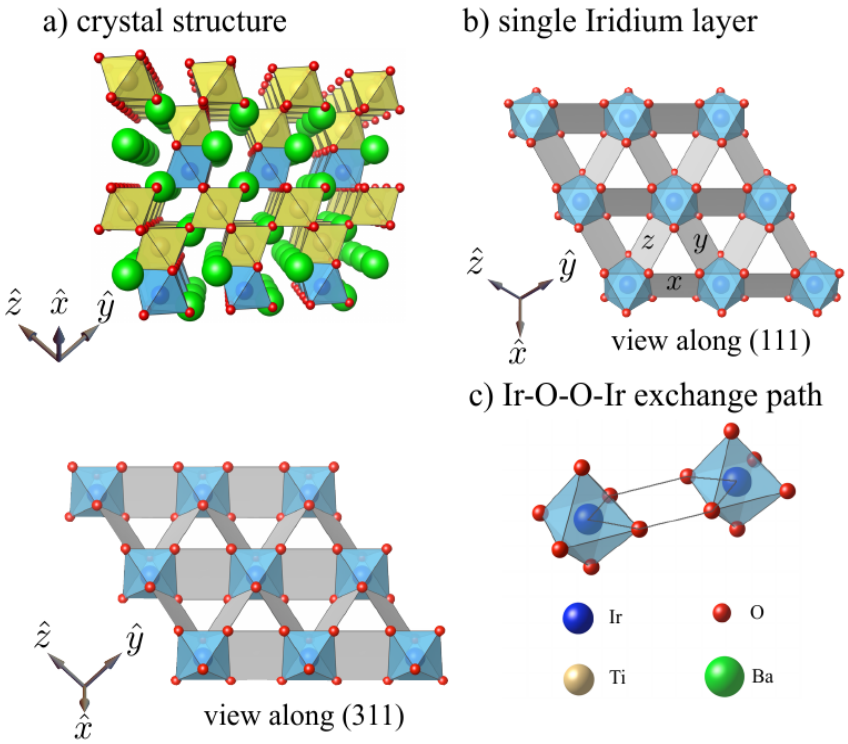

Figure 2.8: Crystal structure of $Ba_3IrTi_2O_9$. The exchange path Ir-O-O-Ir produces direction depended coupling. Figure taken from the paper of M. Becker et al. [6].

2.5.1 Materials

In the recent years there was significant progress in synthesizing new materials. One example is Iridate $Ba_3IrTi_2O_9$ synthesized in 2012 [14]. It shows lack of magnetic ordering down to the temperature of 0.35K, even though large Curie-Weiss temperature $\Theta_{CW} \sim -130$K implies strong magnetic coupling. This could point to a spin liquid ground state. The disorder in the material was quite high, so the results are inconclusive.

It has been argued by M. Becker et al. [6], that this material realizes the Heisenberg-Kitaev model on the triangular lattice. In work done by Andrei Catuneanu et al. [15], it was pointed out that there should be an additional symmetric anisotropic exchange term $\Gamma(S_i^\alpha S_j^\beta + S_i^\beta S_j^\alpha)$ in the effective Hamiltonian. Moreover, it was suggested that Na_xIrO_2 could also realize Heisenberg-Kitaev model on the triangular lattice [5].

Here we will quickly mention how we arrive at the effective Heisenberg-Kitaev model. Details can be found in the cited work. Strong spin-orbit coupling in transition metals with only partially filled d orbitals can lead to an effective j=1/2 states [6, 15]. In particular we have a triangular lattice of isolated Ir^{4+} ions surrounded with octahedral cages of oxygen, as shown in Figure 2.8. The octahedral crystal field splits the Ir^{4+} ions to e_g and t_{2g} orbitals[1].

Strong spin orbit coupling (SOC) then further splits the states into filled effective j=3/2 and half-filled effective j=1/2 states. Strong on site Coulomb repulsion localizes these states.

We want to mention how Kitaev-type interactions come into place, as explained

[1] e_g orbitals consist of d_{z^2} and $d_{x^2-y^2}$ orbitals, whereas t_{2g} orbitals consist of d_{xy},d_{yz} and d_{zx}.

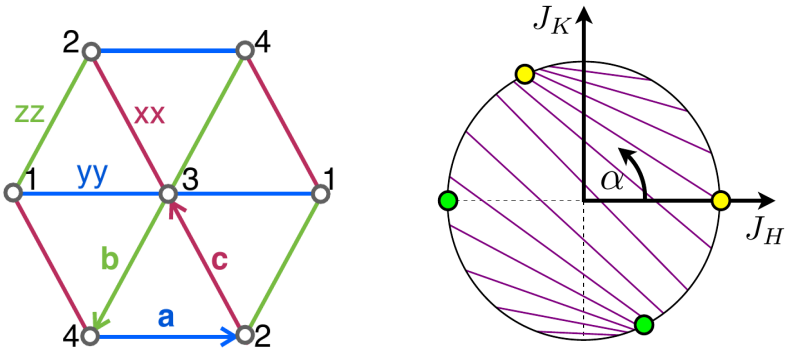

Figure 2.9: Left: labeling of the four sublattices 1-4, figure taken from I. Rousochatzakis et al. [7]. Right: the lines in the figure are connecting Klein dual points. Figure taken from the work done by M. Becker et al. [6].

in M. Becker's PhD thesis. The superexchange spin interaction through a ligand oxygen can happen in two main ways: 180-degree Ir-O-Ir exchange paths give rise to the Heisenberg type interactions, because the same type of orbitals are coupled to the oxygen orbitals. The so called 90-degree Ir-O-Ir exchange paths couple different orbitals, and the two possible paths interfere, resulting in an anisotropic interaction

$$H_{ij}^{90^\circ} = -J_K S_i^\gamma S_j^\gamma. \tag{2.9}$$

The Ir-O-O-Ir exchange path in $Ba_3IrTi_2O_9$ still leads to the destructive interference and suppression of the isotropic exchange. But due to the longer exchange paths, the isotropic part also plays an important role. Thus we arrive at the Heisenberg-Kitaev model on the triangular lattice.

2.5.2 Klein Duality

Duality transformations are a powerful tool in modern physics. The duality transformation between two problems gives information about second problem if we know something about the first problem. In our specific case, we can use a specific transformation, to connect the model at two different couplings ψ. For instance we can deduce the whole phase diagram if we know only the $J_H > 0$ part of it.

The "four sublattice rotation trick" has been know since 2002 [16, 17]. It was generalized by Itamar Kimchi and Ashvin Vishwanath [5], so it can be used for an arbitrary lattice, if the lattice allows for such duality transformation.

We will focus on the triangular lattice. Following the formulation from the work done by Ioannis Rousochatzakis et al. [7], we have labeled four sites in Figure 2.9. The transformation maps the spins $\mathbf{S}$ to the rotated spins $\tilde{\mathbf{S}}$:

$$\mathbf{S_1} = \tilde{\mathbf{S}}_1, \tag{2.10a}$$
$$\mathbf{S_2} = (-\tilde{S}_2^x, -\tilde{S}_2^y, \tilde{S}_2^z), \tag{2.10b}$$
$$\mathbf{S_3} = (-\tilde{S}_3^x, \tilde{S}_3^y, -\tilde{S}_3^z), \tag{2.10c}$$
$$\mathbf{S_4} = (\tilde{S}_4^x, -\tilde{S}_4^y, -\tilde{S}_4^z). \tag{2.10d}$$

The form of Hamiltonian is preserved, with the changed coupling constants (Figure

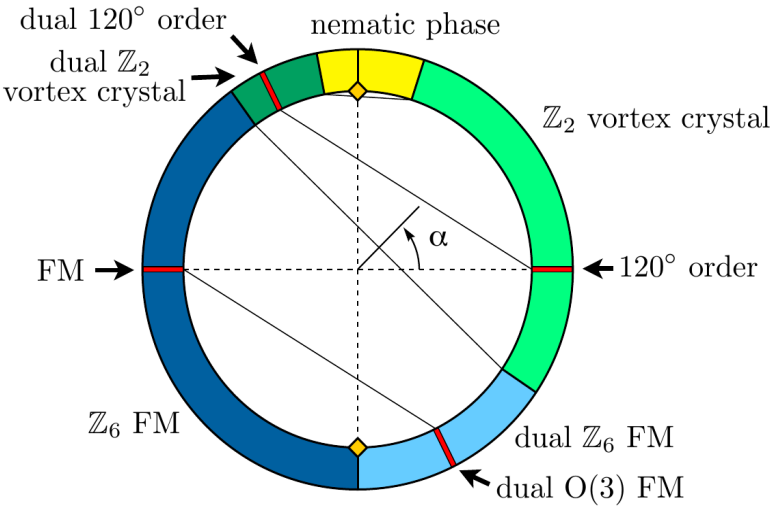

Figure 2.10: Phase diagram obtained from exact diagonalization on small clusters in work done by M. Becker et al. [6], from where this figure is taken.

2.9):

$$J_H \to -J_H, \tag{2.11a}$$

$$J_K \to 2J_H + J_K, \tag{2.11b}$$

$$\psi \to \tilde{\psi} = \arctan\frac{2J_H + J_K}{-J_H} + \pi. \tag{2.11c}$$

In the following analysis we can concentrate on the $J_H > 0$ part of the phase diagram, and later use duality to solve the dual part.

2.5.3 Numerical Results

The classical version of the problem was treated both numerically with Monte Carlo simulations by Ioannis Rousochatzakis et al. [7], and analytically with Luttinger-Tisza approximation by Michael Becker at al. [6].

The quantum problem was treated numerically using exact diagonalization on small clusters of up to 27 sites [6]. The resulting phase diagram is shown in Figure 2.10. In this work M. Becker at al. also examined AF Kitaev point using the density-matrix renormalization group (DMRG) on small clusters. Kazuya Shinjo et al. [18] used the density-matrix renormalization group (DMRG) on lattices with 12 × 6 sites to study the Heisenberg-Kitaev model.

Exact diagonalization on a 12-site cluster and a Schwinger-fermion mean-field method for the point $J_H = 0$, $J_K > 0$ was used by Kai Li et al. [19].

Numerical results point towards the existence of 5 different phases mentioned below.

$\mathbb{Z}_2$ Vortex phase

Classical numerical treatments of the problem suggests that Kitaev coupling close to antiferromagnetic Heisenberg point $\psi = 0$ changes the 120-degree order to an incommensurate non-coplanar $\mathbb{Z}_2$ vortex phase. In the long distance limit a $\mathbb{Z}_2$ vortex phase can be understood as a 120-degree order with a slowly varying coordinate

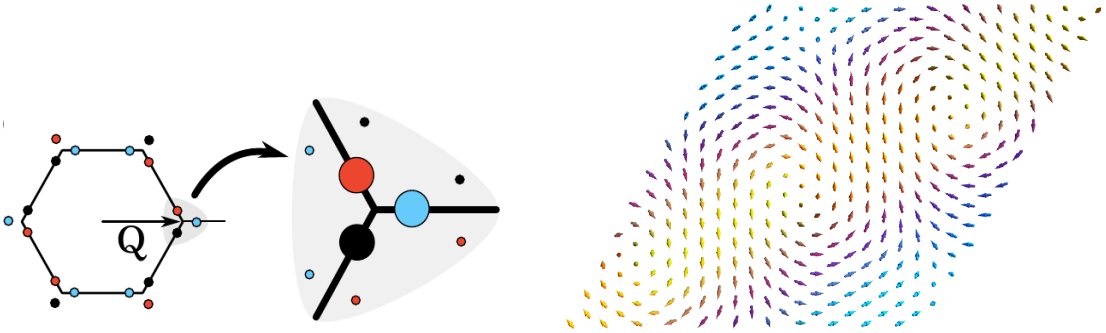

Figure 2.11: Left: Bragg peaks of $S^{\gamma\gamma}(q)$ are shifted. Blue, red and black correspond to γ=x,y and z respectively. Right: One of the three sublattices of the $\mathbb{Z}_2$ vortex crystal. Both figures correspond to the classical model and are taken from the paper of M. Becker et al. [6]

frame. The Bragg peaks in the static spin structure factors[2] $S^{\gamma\gamma}(\mathbf{q})$ are shifted from the corners of BZ to incommensurate momenta in γ direction, as is indicated in Figure 2.11.

What happens in the quantum model is not enteirly clear, DMRG [18] suggests that $S^{\gamma\gamma}(\mathbf{q})$ are not just delta functions, and that $S^{\gamma\gamma}(\mathbf{q})$ are different for different γ.

Nematic Phase

The exact diagonalization data and DMRG point toward the extance of a nematic phase in the vicinity of the Kitaev AF point $\psi = \frac{\pi}{2}$. Classically, the phase at $J_H = 0$, $J_K > 0$ has a large ground state degeneracy consisting of antiferromagnetic Ising chains that are decoupled [7]. Actually, these are not all possible classical ground states, the whole ground state manifold has massive SO(2) degeneracy and can be written as [7]:

$$\mathbf{S_r} = (f_x x_{n-m}(-1)^m, f_y y_m(-1)^n, f_z z_n(-1)^m)^T, \tag{2.12}$$

with $f_x^2 + f_y^2 + f_z^2 = 1$. The lattice coordinates are $(n, m) = n\mathbf{a_x} + m\mathbf{a_y}$ and the sets $\{x_m\}$, $\{y_m\}$ and $\{z_m\}$ are random choices of ± 1. These states contain collinear, coplanar and non-coplanar states.

DMRG suggest that this degeneracy is reduced to non-extensive 3×2^2 [6, 18] and that second nearest AF Ising chains are aligned. This was also shown analytically with quantum order-by-disorder method [20]. Numerical results suggest that for small $J_H > 0$, neighbouring spin chains are aligned antiferromagnetically. Correlations between spins are shown in Figure 2.12.

$\mathbb{Z}_6$ Ferromagnetic Phase

At the FM Heisenberg point $J_K = 0$, $J_H < 0$ the model is SU(2) symmetric, and the ground state consists of spins aligned in the same direction. At this point the ferromagnetic order parameter can point in any direction.

[2] Defined in section 4 with the equation 4.14.

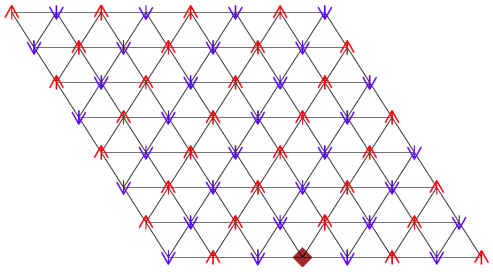

Figure 2.12: $< S_i^x S_j^x >$ for the nematic phase at the Kitaev AF point, the one of the 6 degenerate states that is expected for $J_H > 0$. Upward red (downward blue) arrows correspond to positive (negative) correlations. Figure from [18].

For finite J_K, this degeneracy is reduced to $\mathbb{Z}_6$ by quantum fluctuations, i.e. six directions along the spin axes. This has been shown by quantum order by disorder [7], exact diagonalization and by 1/S term of large S expansion [6].

Effects of finite symmetric anisotropic term Γ.

Andrei Catuneanu et al. [15] tried to explain the physics of $Ba_3IrTi_2O_9$. The theoretical analysis showed that an additional symmetric anisotropic term should be included in the effective Hamiltonian in addition to the Heisenberg-Kitaev part. It can be written as:

$$H_\Gamma = \sum_{\alpha\beta \perp \langle i,j \rangle} \Gamma(S_i^\alpha S_j^\beta + S_i^\beta S_j^\alpha), \tag{2.13}$$

where the sum runs over nearest neighbours. $\alpha\beta \perp \langle i,j \rangle$ means that on γ bond we sum over indices that are different from γ, i.e. on x bond we get a term $\Gamma(S_i^y S_j^z + S_i^z S_j^y)$.

They used Luttinger-Tisza method and classical Monte Carlo simulations to show that a finite value of Γ stabilizes the 120-degree order and stripy phase in a large part of the phase diagram. Specifically, they predict that $Ba_3IrTi_2O_9$ has a stripy ordered ground state.

Chapter 3

Schwinger-boson Mean-field Theory (SBMFT)

Obtaining ground states of the spin Hamiltonians on the triangular lattice is notoriously difficult. Schwinger-boson mean-field theory (SBMFT) provides a way of obtaining an approximate solution to this problem. This is done by representing spin operators with bosons, choosing a mean-field ansatz, preforming the mean-field decoupling and diagonalizing the quadratic Hamiltonian using a Bogoliubov transformation. Mean-field parameters need to be determined self-consistently. The mean-field decoupling has been shown to be equivalent to the large N limit of the symplectic group Sp(N), which is a generalization of SU(2) spin algebra [21].

3.1 Schwinger-bosons Representation

We can express the spin operators with two species $b_\uparrow$ and $b_\downarrow$ of Schwinger-bosons:

$$\mathbf{S_i} = \frac{1}{2} b^\dagger_{i\alpha} \sigma_{\alpha\beta} b_{i\beta}, \tag{3.1}$$

where the indices α and β run over up and down values (we employ a summation convention over the repeated Greek indices), i denotes the lattice site and $\sigma_{\alpha\beta}$ is a vector of Pauli matrices. The commutation relations are preserved, but the resulting Hilbert space is too big. To reobtain the original problem, we need to restrict ourselves to the case where the density of bosons is equal to 2S

$$\hat{n}_i = b^\dagger_{i\alpha} b_{i\alpha} = 2S. \tag{3.2}$$

This is one of the advantages of SBMFT, namely we can formally treat the size of spin as a continuous variable. In the large spin limit $S \to \infty$ we arrive at the classical limit, where we expect a long range ordered phase. By decreasing the spin size, the quantum fluctuations become more and more important. For S small enough (formally it can be smaller than 1/2), the spin liquid phase solutions are obtained. We impose the above constraint by adding a Lagrange multiplier term $\sum_i \lambda_i \left(b^\dagger_{i\alpha} b_{i\alpha} - 2S \right)$ to the Hamiltonian.

The description has a U(1) gauge redundancy:

$$b_{\mathbf{r}\alpha} \to e^{i\phi(\mathbf{r})} b_{\mathbf{r}\alpha}, \tag{3.3a}$$

$$b^\dagger_{\mathbf{r}\alpha} \to e^{-i\phi(\mathbf{r})} b^\dagger_{\mathbf{r}\alpha}. \tag{3.3b}$$

3.2 Operators for Mean-Field Decoupling

Usually, the mean-field decoupling is performed with an order parameter such as magnetization. But spin liquid phase lacks such an obvious choice.

Normal SU(2) symmetric Hamiltonians H_H can be decoupled in terms of SU(2) invariant link operators:

$$\hat{A}_{ij} = \frac{1}{2}\epsilon_{\alpha\beta} b_{i\alpha} b_{j\beta}, \qquad \hat{B}_{ij} = \frac{1}{2} b^{\dagger}_{i\alpha} b_{j\alpha}, \tag{3.4}$$

where i and j are neighbouring lattice sites.

Since our Heisenberg-Kitaev Hamiltonian is not SU(2) invariant, we will also use SU(2) breaking triplet fields $\hat{t}^{\gamma}_{ij}$. The following representation of time reversal operator will be used: $T = -i\sigma^2 K$, where K is complex conjugate operator. We have included factors of (i) in $\hat{t}^{\gamma}$ fields such that they transform only by complex conjugation under time reversal, and the expectation values transform as $T\langle\hat{t}^{\gamma}\rangle = \langle\hat{t}^{\gamma}\rangle^*$. If the expectation value is real, then it is time reversal invariant.

The t^{γ} fields are:

$$\hat{t}^{x}_{ij} = \frac{i}{2}(b_{i\uparrow} b_{j\uparrow} - b_{i\downarrow} b_{j\downarrow}), \qquad \hat{t}^{y}_{ij} = -\frac{1}{2}(b_{i\uparrow} b_{j\uparrow} + b_{i\downarrow} b_{j\downarrow}), \tag{3.5a}$$

$$\hat{t}^{z}_{ij} = -\frac{i}{2}(b_{i\uparrow} b_{j\downarrow} + b_{i\downarrow} b_{j\uparrow}). \tag{3.5b}$$

Note how the change of direction affects the fields:

$$\hat{A}_{ij} = -\hat{A}_{ji}, \qquad \hat{B}_{ij} = \hat{B}^{\dagger}_{ji}, \qquad \hat{t}_{ij} = \hat{t}_{ji}. \tag{3.6}$$

The spin operator terms of the Hamiltonian can now be written as (: : depicts normal ordering):

$$\mathbf{S_i} \cdot \mathbf{S_j} = :\hat{B}^{\dagger}_{ij}\hat{B}_{ij}: - \hat{A}^{\dagger}_{ij}\hat{A}_{ij}, \tag{3.7a}$$

$$S^{\gamma}_i S^{\gamma}_j = -\hat{t}^{\gamma\dagger}_{ij}\hat{t}^{\gamma}_{ij} + :\hat{B}^{\dagger}_{ij}\hat{B}_{ij}:. \tag{3.7b}$$

The equation 3.7 is not an unique way of expressing the Hamiltonian with link operators. Using the appropriate expression is important for the validity of the mean-field approximation. We are now ready to preform a mean-field decoupling. The hat is used to indicate operators.

$$\hat{A}^{\dagger}_{ij}\hat{A}_{ij} = \hat{A}^{\dagger}_{ij}A_{ij} + A^{*}_{ij}\hat{A}_{ij} - |A_{ij}|^2 + (\hat{A}_{ij} - A_{ij})^{\dagger}(\hat{A}_{ij} - A_{ij}), \tag{3.8}$$

where $A_{ij} = \langle\hat{A}_{ij}\rangle$ is the expectation value. We make our first approximation by dropping the last term, i.e. we expand to linear order in fluctuations around the mean-field. Analogously for the other fields.

Our Hamiltonian now reads

$$\begin{aligned} H_{MF} = {} & (J_H + J_K)\sum_{\langle ij\rangle}\Big[(B_{ij})^*\frac{1}{2}b^{\dagger}_{i\alpha}b_{j\alpha} + B_{ij}\frac{1}{2}b_{i\alpha}b^{\dagger}_{j\alpha} - |B_{ij}|^2\Big] \\ & - J_H\sum_{\langle ij\rangle}\Big[(A_{ij})^*\frac{1}{2}\epsilon_{\alpha\beta}b_{i\alpha}b_{j\beta} + A_{ij}\frac{1}{2}\epsilon_{\alpha\beta}b^{\dagger}_{j\beta}b^{\dagger}_{i\alpha} - |A_{ij}|^2\Big] \\ & - J_K\sum_{\gamma||\langle ij\rangle}\Big[(t^{\gamma}_{ij})^*\hat{t}^{\gamma}_{ij} + t^{\gamma}_{ij}(\hat{t}^{\gamma}_{ij})^{\dagger} - |t^{\gamma}_{ij}|^2\Big] + \sum_i \lambda_i\big(b^{\dagger}_{i\alpha}b_{i\alpha} - 2S\big), \end{aligned} \tag{3.9}$$

where the operators $\hat{t}_{ij}^{\gamma}$ defined in the equation 3.5 have still not been explicitly expressed. The resulting Hamiltonian is still too difficult to handle, because we have three parameters for each bond of the lattice. Furthermore, our approach must be self-consistent:

$$A_{ij} = \langle \hat{A}_{ij} \rangle, \qquad B_{ij} = \langle \hat{B}_{ij} \rangle, \qquad t_{ij}^{\gamma} = \langle \hat{t}_{ij}^{\gamma} \rangle, \qquad \frac{\delta F_{MF}}{\delta \lambda_i} = 0. \tag{3.10}$$

These conditions are equivalent to demanding that we are at the saddle point of the free energy $F_{MF}(A_{ij}, B_{ij}, t_{ij}^{\gamma}, \lambda_i)$. Next we focus on the problem of obtaining a mean-field ansatz with the use of the projective symmetry group approach (PSG).

3.3 Search for an Ansatz - PSG

In our treatment we will make second approximation: we demand that the density condition is satisfied only on average: $\lambda \sum_i \left(b_{i\alpha}^{\dagger} b_{i\alpha} - 2S \right)$.

The number of mean-field parameters grows fast with system size, but we expect them to attain just a few different values. Numerical solutions of small clusters agree with this claim [22].

The way out of this, is to demand that the mean-field ansatz is invariant under (at least some) of the symmetries of the original Hamiltonian H. Since our description still has some gauge redundancy, symmetries can act on boson operators $b, b^{\dagger}$ projectively without changing any physical observables.

Systematic way of dealing with the problem of finding ansatzes was introduced by Xiao-Gang Wen for Schwinger-fermion mean-field states [4] called projective symmetry group (PSG) approach. It was later developed for SU(2) invariant Schwinger-boson mean-field ansatzes on triangular lattice by Fa Wang and Ashvin Vishwanath [9] and extended to the time-reversal symmetry-breaking chiral SU(2) invariant ansatzes by Laura Messio et al. [23].

Here we will closely follow the procedure carried out in the literature mentioned above and carefully extend it to non SU(2) symmetric ansatzes.

3.3.1 Gauge Redundancy

In Schwinger-boson representation we have a U(1) gauge redundancy of the description (in contrast to Schwinger-fermion description where it is SU(2)):

$$b_{\mathbf{r}\alpha} \to e^{i\theta(\mathbf{r})} b_{\mathbf{r}\alpha} = G^{\dagger} b_{\mathbf{r}\alpha} G, \tag{3.11a}$$

$$b_{\mathbf{r}\alpha}^{\dagger} \to e^{-i\theta(\mathbf{r})} b_{\mathbf{r}\alpha}^{\dagger} = G b_{\mathbf{r}\alpha}^{\dagger} G^{\dagger}. \tag{3.11b}$$

Where G is the representation of the gauge group action and is given by

$$G = \exp\Big(i \sum_{\mathbf{r}} b_{\mathbf{r}\alpha}^{\dagger} b_{\mathbf{r}\alpha} \theta(\mathbf{r}) \Big). \tag{3.12}$$

This means that our ansatz transforms as

$$A_{ij} \to A_{ij} e^{i(\theta(i)+\theta(j))}, \tag{3.13a}$$

$$B_{ij} \to B_{ij} e^{i(-\theta(i)+\theta(j))}, \tag{3.13b}$$

$$t_{ij}^{\gamma} \to t_{ij}^{\gamma} e^{i(\theta(i)+\theta(j))}. \tag{3.13c}$$

Physical observables are gauge independent, but our ansatz parameters A, B and t are not. So by choosing a specific ansatz we break this gauge symmetry. Actually, the mean-field parameter moduli are related to the scalar product of two spins and are thus physical observables [23]. Other physical observables are the fluxes, which we define as arguments of Wilson loop operators. Relevant examples of Wilson loop operators are $\langle \hat{A}_{ij}\hat{A}^{\dagger}_{jk}\hat{A}_{kl}\hat{A}^{\dagger}_{li}\rangle$, $\langle \hat{B}_{ij}\hat{B}_{jk}\hat{B}_{ki}\rangle$ and $\langle \hat{A}_{ij}\hat{A}^{\dagger}_{jk}\hat{t}_{kl}\hat{A}^{\dagger}_{li}\rangle$. This information will be later used to distinguish different ansatzes.

We define the invariant gauge group (**IGG**) as the **set of gauge transformations that do not modify a specific ansatz**. IGG must be at least the $\mathbb{Z}_2$ group formed by elements $\theta(i) = 0$ and $\theta(i) = \pi$ for all lattice sites. In some cases it can be a bigger group. One example of a U(1) IGG would be nearest neighbour coupled spins on a bipartite lattice without a B_{ij} field. Then the elements of IGG are of the form $\theta(i) = \pm\theta$, where we have a + sign on one sublattice and a - sign on the other with some angle θ.

3.3.2 Projective Symmetry Group (PSG)

Imagine that we have a group of symmetries $\mathcal{X}$ with elements X of our original Hamiltonian. In works [4, 9, 23], which we closely follow, this is the group of lattice symmetries. But in our non-SU(2) invariant case, this symmetry can also act as a rotation on the spin part, which is expressed in terms of the axis of rotation and an angle that depends on the symmetry X as $\hat{\theta}(X)$:

$$X : \begin{bmatrix} b^{\dagger}_{\mathbf{r}\uparrow} \\ b^{\dagger}_{\mathbf{r}\downarrow} \end{bmatrix} \rightarrow e^{-\frac{i}{2}\hat{\theta}(X)\sigma} \begin{bmatrix} b^{\dagger}_{X(\mathbf{r})\uparrow} \\ b^{\dagger}_{X(\mathbf{r})\downarrow}, \end{bmatrix} \tag{3.14}$$

with $\sigma = (\sigma^x, \sigma^y, \sigma^z)^T$ being vector of Pauli matrices.

X acts on the ansatz as:

$$A_{ij} \rightarrow A_{X(i)X(j)}, \qquad B_{ij} \rightarrow B_{X(i)X(j)}, \qquad t^{\gamma}_{ij} \rightarrow t^{X(\gamma)}_{X(i)X(j)}. \tag{3.15}$$

Transformation of t fields is in general complicated, since we get some nontrivial combinations of b and $b^{\dagger}$. The expression written here is only valid for our specific model and its symmetries. Since the A and B fields are SU(2) invariant, rotations in spin space do not affect them.

Usually we demand that if our ansatz satisfies the symmetries, it should get back to itself by acting with the symmetry. But, having the gauge redundancy, it is enough to demand that the ansatz is transformed to a gauge equivalent ansatz. Then there exists a gauge transformation G_X, such that combined transformation $G_X X$ acts as the identity on the ansatz.

The **set of all transformation $G_X X$ that leave a mean-field ansatz invariant** is called the Projective Symmetry Group (**PSG**) [4].

Obviously, IGG is a subset of PSG, that consists only of gauge transformations and thus correspond to $1 \in \mathcal{X}$. Thus for each element X of $\mathcal{X}$, if $G_X X \in$ PSG then also $G_I G_X X \in$ PSG for any element $G_I \in$ IGG. It follows that:

$$\text{PSG} \cong \text{IGG} \times X \tag{3.16}$$

The PSG depends only on imposed symmetries $\mathcal{X}$ and on the ansatz, but not directly on Hamiltonian. That is one of the main reasons why the PGS approach is so powerful.

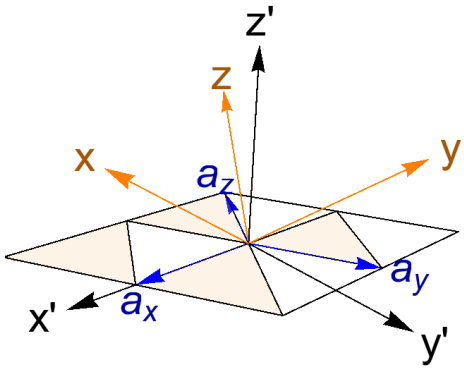

Figure 3.1: Fixing the spin space axis to real space. The spin operator S^γ acts along the γ direction. The C_3 rotation rotates around z' axis. Translations by the lattice vectors a_x and a_y are generated by T_1 and T_2.

3.3.3 Symmetries

To find the algebraic constraints on PSG, we first need to examine the symmetries of our Hamiltonian. The situation is a bit more complicated than in the SU(2) symmetric case, since we need to be careful about how symmetries act on the spin space, and how bosonic operators $b_{\mathbf{r}\alpha}$ transform as spinors.

We have mentioned the point group symmetries of our problem before in section 2.4. Our ansatz has to incorporate the following symmetries:

- Translations along the two independent lattice directions $\mathbf{a_x}$ and $\mathbf{a_y}$ generated by T_1 and T_2,
- D_{3d} point group.
- We will not explicitly demand time reversal symmetry, but we will later discuss it.

Rotations in spin space act trivially on SU(2) invariants and non-trivially on t^γ. Generators of the symmetries act as:

$$T_1 : (r_1, r_2) \to (r_1 + 1, r_2), \tag{3.17a}$$
$$T_2 : (r_1, r_2) \to (r_1, r_2 + 1), \tag{3.17b}$$
$$S_6 : (r_1, r_2; S_x, S_y, S_z) \to (r_1 - r_2, r_1; -S_y, -S_z, -S_x), \tag{3.17c}$$
$$C_3 : (r_1, r_2; S_x, S_y, S_z) \to (-r_2, r_1 - r_2; S_z, S_x, S_y), \qquad S_6^2 = C_3, \tag{3.17d}$$
$$\sigma_v : (r_1, r_2; S_x, S_y, S_z) \to (r_2, r_1; S_y, S_x, S_z), \tag{3.17e}$$

$$C_3 : \begin{bmatrix} b^\dagger_{(r_1,r_2)\uparrow} \\ b^\dagger_{(r_1,r_2)\downarrow} \end{bmatrix} \to e^{-\frac{i}{2\sqrt{3}}\frac{2\pi}{3}(\sigma^x+\sigma^y+\sigma^z)} \begin{bmatrix} b^\dagger_{(-r_2,r_1-r_2)\uparrow} \\ b^\dagger_{(-r_2,r_1-r_2)\downarrow} \end{bmatrix}, \tag{3.17f}$$

with the notation $(r_1, r_2) = r_1\mathbf{a_x} + r_2\mathbf{a_y}$ and S_6 denotes the generator of six-fold pseudorotation in D_{3d}. Translations act trivially on spin space.

We can check how C_3 acts on t^γ fields and see that they indeed act as expected (that is also the reason why we have inserted the factors of (i) and -1 in fields $\hat{t}^\gamma$ the way we did):

$$C_3(t^x) = t^y, \quad C_3(t^y) = t^z, \quad C_3(t^z) = t^x. \tag{3.18}$$

3.3.4 The Algebraic Projective Symmetry Groups

We want to find all ansatzes compatible with the imposed symmetries of the model. First we find the algebraic PSG's [4, 9, 23], then we look for all ansatzes consistent with an algebraic PSG and specific problem. Algebraic PSG's are determined only by the chosen symmetry group $\mathcal{X}$ and the chosen IGG.

The basic idea is that the algebraic relations of the generators of $\mathcal{X}$ impose algebraic relations on the PSG. There are only finitely many of them, since every symmetry element can be rewritten as a "normal ordered" product of generators by using these constraints. For example, consider the translations T_1 and T_2. The algebraic relation on $\mathcal{X}$ is

$$T_2^{-1}T_1^{-1}T_2T_1 = I. \tag{3.19}$$

When implemented by the PSG, we see:

$$(G_{T_2}T_2)^{-1}(G_{T_1}T_1)^{-1}G_{T_2}T_2G_{T_1}T_1 \in \text{IGG}. \tag{3.20}$$

Using $T_1T_2 = T_2T_1$ and $T_1T_1^{-1} = 1$ the expression can be rewritten as:

$$G_{T_2}^{-1}(T_1^{-1}G_{T_1}^{-1}T_1)(T_1^{-1}G_{T_2}T_1)(T_1^{-1}T_2G_{T_1}(T_1^{-1}T_2)^{-1}) = \pm 1. \tag{3.21}$$

The combination $Y^{-1}G_XY$ applied to site $\mathbf{r}$ will just act as the gauge transformation on the site $Y(\mathbf{r})$. Since translations do not act on spin space, and the gauge transformation G_X just change $b_\mathbf{r} \to b_\mathbf{r}e^{i\phi_X(\mathbf{r})}$ we end up with (all equations concerning phases hold up to 2π)

$$-\phi_{T_2}[\mathbf{r}] - \phi_{T_1}[T_1(\mathbf{r})] + \phi_{T_2}[T_1(\mathbf{r})] + \phi_{T_1}[T_2^{-1}T_1(\mathbf{r})] = p_1\pi. \tag{3.22}$$

We will now fix the gauge as in Wen's original paper on fermionic PSG [4].

If we perform a gauge transformation G on $G_XX \in$ PSG, the ansatz is invariant under $\tilde{G}_XX$:

$$G(G_XX)G^{-1} = (GG_XXG^{-1}X^{-1})X, \tag{3.23a}$$

$$G_X \to \tilde{G}_X = (GG_XXG^{-1}X^{-1}). \tag{3.23b}$$

So the phases change as:

$$\phi_X[\mathbf{r}] \to \phi_G[\mathbf{r}] + \phi_X[\mathbf{r}] - \phi_G[X^{-1}(\mathbf{r})]. \tag{3.24}$$

We partially fix the gauge

$$\phi_G[\mathbf{r}] - \phi_G[T_1^{-1}(\mathbf{r})] = \phi_{T_1}[\mathbf{r}], \tag{3.25}$$

so the new G_{T_1} is trivial, i.e. $\phi_{T_1}(\mathbf{r}) = 0$. Equation 3.22 becomes:

$$\phi_{T_2}[T_1(\mathbf{r})] - \phi_{T_2}[\mathbf{r}] = p_1\pi. \tag{3.26}$$

We can also fix $\phi_{T_2}(r_1, 0) = 0$, since the previous gauge fixing only fixed the gauge in the direction of T_1. Translational invariance thus leads to:

$$\phi_{T_1}(r_1, r_2) = 0, \qquad \phi_{T_2}(r_1, r_2) = p_1 \pi r_1. \tag{3.27}$$

The gauge is still not totally fixed, since

$$G_1 : \ \phi(\mathbf{r}) = \text{constant}, \tag{3.28a}$$
$$G_2 : \ \phi(\mathbf{r}) = \pi r_1, \tag{3.28b}$$
$$G_3 : \ \phi(\mathbf{r}) = \pi r_2. \tag{3.28c}$$

do not interfere with the previous gauge fixing. We use G_1 to fix $A_{(0,0)\to(1,0)}$ to be real.

The chiral PSG's - weakly symmetric states

Upon condensation of bosons in the limit $S \to \infty$ we arrive at the classical ground states of spin Hamiltonians. It has been shown that using only strictly symmetric (time reversal symmetric) ansatzes misses the chiral (non coplanar) classical ground states [23]. So a more general approach is needed, where time reversal symmetry and some lattice symmetries can be broken.

Weakly symmetric ansatzes are the ones that respect all symmetries up to time reversal [23], and are extension of strictly symmetric ansatzes to chiral ones.

It is important to note the distinction between even and odd symmetries (parity $\epsilon_X = \pm 1$). We will see the parity of the transformation by examining the transformation of fluxes. But first, let's look closely at the subgroup of symmetries that are necessarily even, $\mathcal{X}_e \in \mathcal{X}$. It necessarily contains the squares of elements since $\epsilon_X^2 = 1$, but it may contain more elements.

Chiral algebraic PSG's of $\mathcal{X}$ are defined as the algebraic PSG's of $\mathcal{X}_e$ [23]. The transformations that may be odd are contained in $\mathcal{X}_0 = (\mathcal{X} - \mathcal{X}_e)$. We will determine all weakly symmetric ansatzes, by examining the transformations of $\mathcal{X}_0$ on the fluxes of the ansatzes compatible with chiral algebraic PSGs.

The group of necessarily even symmetries $\mathcal{X}_e$ necessarily contains squares of the generators $T_1^2, T_2^2, S_6^2 = C_3$. To determine the rest of the elements, we first list the algebraic relations in $\mathcal{X}$:

$$T_2^{-1} T_1^{-1} T_2 T_1 = I, \tag{3.29a}$$
$$\sigma_v^2 = I, \tag{3.29b}$$
$$S_6^6 = I, \tag{3.29c}$$
$$S_6^{-1} T_1 S_6 T_2 = I, \tag{3.29d}$$
$$T_2 S_6 = S_6 T_1 T_2, \tag{3.29e}$$
$$T_1 \sigma_v = \sigma_v T_2, \tag{3.29f}$$
$$S_6 \sigma_v S_6 = \sigma_v. \tag{3.29g}$$

The only difference in our derivation compared to [23] is that we have a pseudo rotation generator S_6 that also acts on the spin space instead of just normal rotation on the lattice. But at this step, this does not make any real difference. From the

above equations we can get some more information on the parity ϵ of the transformations:

$$\epsilon_{T_1}\epsilon_{S_6} = \epsilon_{S_6}\epsilon_{T_2}, \tag{3.30a}$$
$$\epsilon_{T_2}\epsilon_{S_6} = \epsilon_{S_6}\epsilon_{T_1}\epsilon_{T_2}. \tag{3.30b}$$

Thus $\epsilon_{T_1} = \epsilon_{T_2} = 1$ and $\mathcal{X}_e$ is generated by T_1, T_2 and C_3. It has the following algebraic relations:

$$T_2^{-1}T_1^{-1}T_2T_1 = I, \tag{3.31a}$$
$$C_3^3 = I, \tag{3.31b}$$
$$C_3T_1C_3^{-1}T_2^{-1} = I, \tag{3.31c}$$
$$C_3^{-1}T_2^{-1}T_1^{-1} = T_2C_3^{-1}. \tag{3.31d}$$

From above, we obtain the algebraic constraints on phases:

$$\phi_{T_1}(r_1, r_2) = 0, \tag{3.32a}$$
$$\phi_{T_2}(r_1, r_2) = p_1\pi r_1, \tag{3.32b}$$
$$\phi_{C_3}(r_1, r_2) + \phi_{C_3}(C_3(r_1, r_2)) + \phi_{C_3}(C_3^2(r_1, r_2)) = p_2\pi, \tag{3.32c}$$
$$-\phi_{T_2}(r_1, r_2) - \phi_{C_3}(T_2^{-1}(r_1, r_2)) + \phi_{C_3}(r_1, r_2) = p_3\pi, \tag{3.32d}$$
$$\phi_{T_2}(T_1^{-1}(r_1, r_2)) + \phi_{C_3}(T_2^{-1}T_1^{-1}(r_1, r_2)) - \phi_{C_3}(r_1, r_2) + \phi_{T_2}(T_2C_3^2(r_1, r_2)) = p_4\pi. \tag{3.32e}$$

We finally completely fix the gauge by using G_3 to set $p_3 = 0$ and G_2 to set $p_4 = 0$.

On the triangular lattice, which has one site per lattice cell we obtain (equation 3.32c) the condition that allows us to simplify above equations to:

$$\phi_{T_1}(r_1, r_2) = 0 \tag{3.33a}$$
$$\phi_{T_2}(r_1, r_2) = p_1\pi r_1 \tag{3.33b}$$
$$\phi_{C_3}(r_1, r_2) = p_1\left(r_2 - \frac{r_1 + 1}{2}\right) + \frac{k\pi}{3} \tag{3.33c}$$

with $p_1 = 0, 1$ and $k = \pm p_2 = -1, 0, 1$.

Now we search for all ansatzes of our decoupling consistent with $\mathcal{X}_e$. We have already fixed $A_{(0,0)\to(1,0)} = A$ to be real. Further, we fix the bonds $t^x_{(0,0)\to(1,0)} = te^{i\phi_t}$ and $B_{(0,0)\to(1,0)} = Be^{i\phi_B}$. All other bonds can be deduced using PSG. The result is presented in Figure 3.2. If $p_1 = 1$ the unit cell is doubled and the treatment of the problem is more cumbersome.

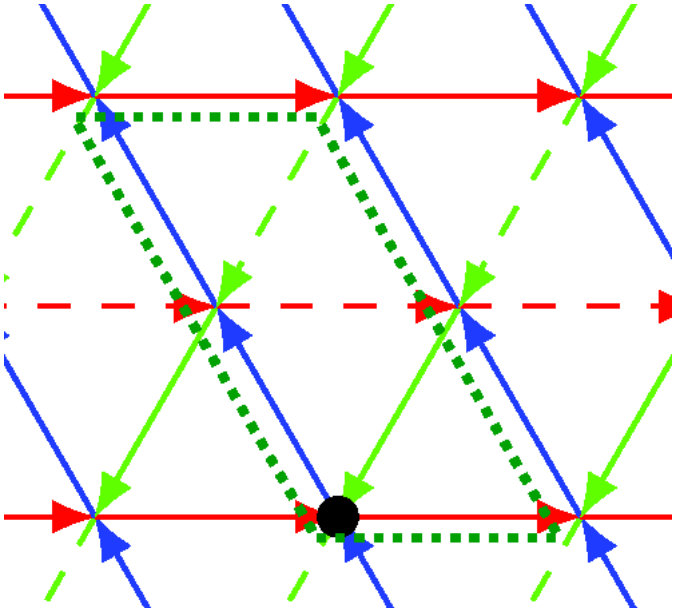

Figure 3.2: Ansatzes respecting the symmetries on the triangular lattice. All arrows carry B_{ij} parameters of modulus B and argument ϕ_B, A_{ij} parameters of modulus A and argument 0 on red arrows, $k\frac{2\pi}{3}$ on blue ones and $k\frac{4\pi}{3}$ on green ones. t^γ fields have amplitude t on γ bonds and phases $\phi_t + k\frac{2\pi}{3}n(\gamma)$ where $n(\gamma)$ is 0,1,2 on red, blue and green arrows. On dashed arrows, A_{ij}, t_{ij} and B_{ij} take an extra $p_1\pi$ phase. The figure is taken from the paper written by Laura Messio et al. [23], and the information about t fields has been added.

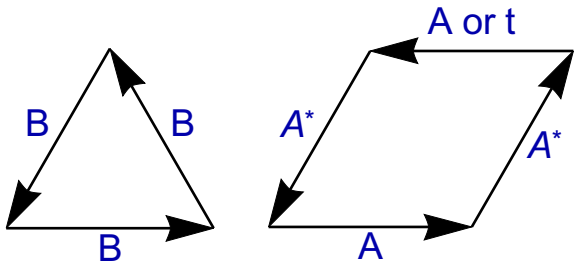

Figure 3.3: Fluxes used to determine the additional constraints. Depending on the position and orientation of the bonds, there are additional phase factors, as explained in Figure 3.2.

Transformations of Fluxes

Until now, we have taken into account only the symmetries $\mathcal{X}_e$. The rest of the symmetries $\mathcal{X}_0$ will be investigated using transformations of fluxes.

In the addition to fluxes $\mathrm{Arg}(A_{ij}A^*_{jk}A_{kl}A^*_{li})$ and $\mathrm{Arg}(B_{ij}B_{jk}B_{ki})$ used in [23], we use an additional independent flux $\mathrm{Arg}(A_{ij}A^*_{jk}t_{kl}A^*_{li})$. The fluxes are shown in Figure 3.3. Transformations under pseudo-rotation S_6 and reflection σ_v give some new constraints:

$$2k\pi(1-\epsilon_{S_6})/3 = 0, \tag{3.34a}$$
$$2k\pi(1+\epsilon_{\sigma_v})/3 = 0, \tag{3.34b}$$
$$\phi_B(1+\epsilon_{S_6}) = p_1\pi, \tag{3.34c}$$
$$\phi_B(1-\epsilon_{\sigma_v}) = p_1\pi, \tag{3.34d}$$
$$\phi_t(1-\epsilon_{S_6}) = 0, \tag{3.34e}$$
$$\phi_t(1-\epsilon_{\sigma_v}) = 0. \tag{3.34f}$$

The equations 3.34e and 3.34f are our new addition in comparison with the paper [23] written by L. Messio et al. For different parities we get the following results:

ϵ_{S_6}	ϵ_{σ_v}	p_1	k	ϕ_B	ϕ_t
1	1	0	0	0,π	any
-1	-1	0	0	0,π	0,π
1	-1	0,1	-1,0,1	$p_1\pi/2, p_1\pi/2+\pi$	0,π
-1	1	0	0	any	0,π

The time reversal operator acts on the ansatzes only by complex conjugation (we have specifically chosen such $\hat{t}^\gamma_{ij}$ operators). Nonzero expectation value of t fields break the SU(2) symmetry of the problem, so the only totally symmetric ansatz is the one with $p_1 = 0$, $k = 0$ and $\phi_t = 0$. In the following we will focus mostly on this ansatz.

If we allow for negative fields, then phases 0 and π correspond to the same ansatz. The list of all possible weakly symmetric ansatzes is shown in Table 3.1

Ansatz	p_1	k	ϕ_B	ϕ_t
1	0	0	0	0
2	0	0	0	any
3	0	0	any	0
4	0	-1,1	0	0
5	1	0	$\pi/2$	0
6	1	-1,1	$\pi/2$	0

Table 3.1: Summary of all possible weakly symmetric PSG's. Here we allow for negative fields so phases 0 and π correspond to the same ansatz. Ansatz 1 respect all symmetries in $\mathcal{X}$ and also time reversal, ansatz 2 breaks time reversal symmetry, but all symmetries in $\mathcal{X}$ are even. Ansatzes 3-6 are weakly symmetric and correspond to chiral states. Moreover, ansatzes with $p_1 = 1$ have a doubled unit cell.

Chapter 4

Treatment of the Totally Symmetric Ansatz

In this chapter we will investigate the totally symmetric ansatz, which is characterized with $p_1 = 0$, $k = 0$, $\phi_b = 0$ and $\phi_t = 0$. We will derive how to determine the mean-field parameters self-consistently. Furthermore, we will explain how to calculate characteristic quantities: one spinon dispersion and static spin structure factor.

4.1 Fourier Transformation

After we have selected the ansatz, we can preform a Fourier transformation to simplify H_{MF}. We will use the following definition of the Fourier Transformation:

$$b_{i\alpha} = \frac{1}{\sqrt{N}} \sum_{\mathbf{k}} e^{-i\mathbf{k}\mathbf{r_i}} b_{\mathbf{k}\alpha}, \qquad b_{k\alpha} = \frac{1}{\sqrt{N}} \sum_{\mathbf{r_i}} e^{i\mathbf{k}\mathbf{r_i}} b_{\mathbf{i}\alpha}. \tag{4.1}$$

The normalization of δ is thus

$$\sum_{\mathbf{r_i}} e^{i(\mathbf{k}-\mathbf{k_0})\mathbf{r_i}} = \delta_{k,k_0} N. \tag{4.2}$$

With the use of the ansatz, we simplify our H_{MF} by going to momentum space. A detailed calculation is presented in Appendix A.1. We rewrite our H_{MF} using the Nambu spinor $\Psi_{\mathbf{k}} = (b_{\mathbf{k}\uparrow}, b_{\mathbf{k}\downarrow}, b^\dagger_{-\mathbf{k}\uparrow} b^\dagger_{-\mathbf{k}\downarrow})^T$. The density term can be expressed as follows:

$$\begin{aligned} \sum_i b^\dagger_{i\alpha} b_{i\alpha} &= \sum_{\mathbf{k}} b^\dagger_{\mathbf{k}\alpha} b_{\mathbf{k}\alpha} = \frac{1}{2} \sum_{\mathbf{k}} (b^\dagger_{\mathbf{k}\alpha} b_{\mathbf{k}\alpha} + b^\dagger_{-\mathbf{k}\alpha} b_{-\mathbf{k}\alpha}) \\ &= \frac{1}{2} \sum_{\mathbf{k}} (b^\dagger_{\mathbf{k}\alpha} b_{\mathbf{k}\alpha} + b_{-\mathbf{k}\alpha} b^\dagger_{-\mathbf{k}\alpha}) - \frac{2N}{2}, \end{aligned} \tag{4.3}$$

where we used the commutation relations $\left[b_{k\alpha}, b^\dagger_{k'\beta}\right] = \delta_{k,k'}\delta_{\alpha\beta}$ to get the form of the Nambu spinor, the factor of two comes from the two species of bosons $\uparrow$ and $\downarrow$. We write H_{MF} as:

$$\frac{1}{N} H_{MF} = \frac{1}{N} \sum_{\mathbf{k}} \psi^\dagger_{\mathbf{k}} H_{\mathbf{k}} \psi_{\mathbf{k}} + 3J_H |A|^2 + 3J_K |t|^2 - 3(J_H + J_K)|B|^2 - \lambda(1 + 2S). \tag{4.4}$$

For our totally symmetric ansatz, the matrix $H_{\mathbf{k}}$ has the following form:

$$\begin{aligned}
H_{ii} &= \frac{\lambda}{2} + \frac{(J_H + J_K)}{2} B(\cos(k_1) + \cos(k_2) + \cos(k_3)), \\
H_{14} &= \frac{1}{2}(iJ_H A(\sin(k_1) + \sin(k_2) + \sin(k_3)) - iJ_K t\cos(k_3)), \\
H_{23} &= \frac{1}{2}(-iJ_H A(\sin(k_1) + \sin(k_2) + \sin(k_3)) - iJ_K t\cos(k_3)), \\
H_{13} &= \frac{J_K}{2}(i\ t\cos(k_1) - t\cos(k_2)), \\
H_{24} &= \frac{J_K}{2}(-i\ t\cos(k_1) - t\cos(k_2)),
\end{aligned} \tag{4.5}$$

$$\begin{aligned}
&H_{32} = H_{23}^*, && H_{41} = H_{14}^*, && H_{31} = H_{13}^*, && H_{42} = H_{24}^*, \\
&H_{12} = 0, && H_{21} = 0, && H_{34} = 0, && H_{43} = 0.
\end{aligned}$$

With $k_1 = \mathbf{k}\cdot\mathbf{a_x} = k_x$, $k_2 = \mathbf{k}\cdot\mathbf{a_y} = -\frac{1}{2}k_x + \frac{\sqrt{3}}{2}k_y$ and $k_3 = -k_1 - k_2$.

4.2 Bogoliubov Transformation

After mean-field decoupling, we are left with a quadratic Hamiltonian, which can be diagonalized by a Bogoliubov transformation using a SU(2,2) transformation matrix $P_{\mathbf{k}}$ defined via:

$$\Psi_{\mathbf{k}} = (b_{\mathbf{k}\uparrow}, b_{\mathbf{k}\downarrow}, b^\dagger_{-\mathbf{k}\uparrow} b^\dagger_{-\mathbf{k}\downarrow})^T, \tag{4.6a}$$

$$\Gamma_{\mathbf{k}} = (\gamma_{\mathbf{k}1}, \gamma_{\mathbf{k}2}, \gamma^\dagger_{-\mathbf{k}1}\gamma^\dagger_{-\mathbf{k}2})^T, \tag{4.6b}$$

$$\Psi_{\mathbf{k}} = P_{\mathbf{k}}\Gamma_{\mathbf{k}}, \tag{4.6c}$$

where the $\gamma_{\mathbf{k}i}$ operators describe bosonic Bogoliubov quasiparticles, i.e. bosonic spinons carrying spin 1/2. We need to find matrices $P_{\mathbf{k}}$ and a diagonal matrix $\Omega_{\mathbf{k}}$ such that:

$$P^\dagger_{\mathbf{k}} H_{\mathbf{k}} P_{\mathbf{k}} = \Omega_{\mathbf{k}}, \qquad\qquad P^\dagger_{\mathbf{k}} \tau^z P_{\mathbf{k}} = \tau^z, \tag{4.7}$$

with $\tau^z = \mathrm{diag}(1, 1, -1, -1)$. The second condition is necessary to maintain the commutation relations in the new variables. From this follows:

$$P^{-1}_{\mathbf{k}} \left(\tau^z H_{\mathbf{k}}\right) P_{\mathbf{k}} = \tau^z \Omega_{\mathbf{k}} \tag{4.8}$$

We have diagonalized the matrix $\tau^z H_{\mathbf{k}}$ using computer software and obtained a diagonal matrix $\Omega_{\mathbf{k}}$ with two different eigenvalues that are twice degenerate. To get the transformation matrix $P_{\mathbf{k}}$ in the right form, we needed to be careful with the order of the rows and normalization. Since we diagonalized the problem, our vacuum is annihilated by $\gamma_{\mathbf{k}}$:

$$\gamma_{\mathbf{k}\alpha}|\mathrm{GS}\rangle = 0. \tag{4.9}$$

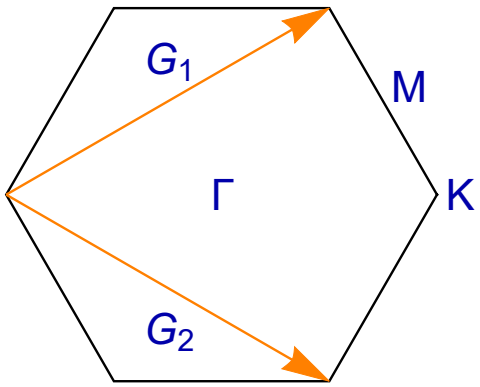

Figure 4.1: First Brillouin zone of the triangular lattice. Reciprocal primitive vectors $\mathbf{G_1}$ and $\mathbf{G_2}$ as well as position of Γ, M and K points are shown.

The eigenvalues correspond to half of the spinon excitation energy and take the form:

$$\omega_{1,2}(\mathbf{k}) = \frac{1}{2}\sqrt{\begin{array}{l}\left(\lambda + (J_H + J_K)\tilde{B}\right)^2 - J_H^2\tilde{A}^2 - J_K^2 t^2(\cos^2 k_1 + \cos^2 k_2 + \cos^2 k_3) \\ \mp 2|J_H J_K \tilde{A}|\sqrt{t^2(\cos^2 k_1 + \cos^2 k_2 + \cos^2 k_3)}\end{array}}, \tag{4.10}$$

$$\begin{aligned}\tilde{A} &= A(\sin(k_1) + \sin(k_2) + \sin(k_3)),\\ \tilde{B} &= B(\cos(k_1) + \cos(k_2) + \cos(k_3)).\end{aligned}$$

We again used the notation $k_1 = \mathbf{k}\cdot\mathbf{a_x}$, $k_2 = \mathbf{k}\cdot\mathbf{a_y}$ and $k_3 = -k_1 - k_2$.

Since the order of $\gamma_{\mathbf{k}}$ is reversed in front of the last two eigenvalues, we use the commutation relations and $\frac{1}{N}H_{MF}$ becomes:

$$\begin{aligned}\frac{1}{N}H_{MF} = \frac{1}{N}\sum_{\mathbf{k}}\left(2\omega_1(\mathbf{k})\gamma^\dagger_{\mathbf{k}1}\gamma_{\mathbf{k}1} + 2\omega_2(\mathbf{k})\gamma^\dagger_{\mathbf{k}2}\gamma_{\mathbf{k}2}\right) + \frac{1}{N}\sum_{\mathbf{k}}\left(\omega_1(\mathbf{k}) + \omega_2(\mathbf{k})\right)\\ + 3J_H|A|^2 + 3J_K|t|^2 - 3(J_H + J_K)|B|^2 - \lambda(1 + 2S).\end{aligned} \tag{4.11}$$

The thermodynamic limit is taken and summation is replaced by integration. The measure can be deduced from

$$1 = \frac{1}{N_{sites}}\sum_{\mathbf{k}} = \frac{1}{\mathrm{Vol}_{BZ}}\int_{BZ}\mathrm{d}^2k, \tag{4.12}$$

where $\int_{BZ}$ denotes the integration over the first Brillouin zone, which is a hexagon and is shown in Figure 4.1.

4.3 Satisfying the Self-Consistency Relations

We need to determine the values of the mean-field parameters in order to satisfy self-consistency equations. This is equivalent to finding the saddle points of the free energy $F_{MF}(A, B, t, \lambda)$ and in our case the mean-field energy of the ground state,

which can be easily shown by demanding that the first derivatives of $F_{MF}(A, B, t, \lambda)$ vanish. The ground state energy reads:

$$\frac{E_{MF}}{N} = \int_{BZ} \frac{\mathrm{d}^2 k}{\mathrm{Vol}_{BZ}} \big(\omega_1(\mathbf{k}) + \omega_2(\mathbf{k})\big) + 3J_H|A|^2 + 3J_K|t|^2 - 3(J_H + J_K)|B|^2 - \lambda(1 + 2S). \tag{4.13}$$

For this task we use Mathematica. Because we need to compute the energy at many different points, it is important to optimize the program.

The integration over the first Brillouin zone is the most costly operation. This is why we used fast Cuhre integration routine from Cuba package [24]. It was considerably faster than all Mathematica's integration routines.

In our case we found the relevant saddle point by maximizing E_{MF} with respect to B and λ and minimizing with respect to A and t. We tried different routines, and ended up using Mathematica's FindMaximum and FindMinimum functions. These are searching only for local maximum/minimum, which we checked that was also the global one by using different starting values.

It can happen that by decreasing λ, eigenvalues become complex at some momenta before E_{MF} reaches a local maximum. This means that the excitation gap closes at some momenta and a Bose-Einstein condensate is formed leading to a state with long-range magnetic order. In this case λ is set by the point where the eigenvalues become complex (for some momenta).

To further speed up the program, we tested if the eigenvalues are real at the momenta, where the minima is most probable to occur, i.e. Γ, M and K points. If the eigenvalue was complex, we did not need to perform the integration.

4.4 Static Spin Structure Factor

We want to characterise resulting states. To accomplish this, it is illustrative to compute the static spin structure factor and its components. They are the Fourier transform of correlation functions $\langle S^c(0) S^d(\mathbf{r})\rangle$ and can be measured experimentally by neutron scattering experiments.

$$S(\mathbf{q}) = \frac{1}{N} \sum_{i,j} \langle \mathrm{GS}|\mathbf{S_i} \cdot \mathbf{S_j}|\mathrm{GS}\rangle e^{i\mathbf{q}(\mathbf{r_i} - \mathbf{r_j})} = S^{xx}(\mathbf{q}) + S^{yy}(\mathbf{q}) + S^{zz}(\mathbf{q}). \tag{4.14}$$

In addition we compute off-diagonal elements of the spin correlation tensor

$$S^{ab}(\mathbf{q}) = \frac{1}{N} \sum_{i,j} \langle \mathrm{GS}|S_i^a S_j^b|\mathrm{GS}\rangle e^{i\mathbf{q}(\mathbf{r_i} - \mathbf{r_j})}. \tag{4.15}$$

We express the terms using Schwinger-bosons:

$$S^{cd}(\mathbf{q}) = \frac{1}{4N^3} \sum_{i,j,\mathbf{k},\mathbf{k'},\mathbf{k''},\mathbf{k'''}} \langle b^\dagger_{\mathbf{k}\alpha} \sigma^c_{\alpha\beta} b_{\mathbf{k'}\beta} e^{i\mathbf{r_i}(\mathbf{k} - \mathbf{k'} + \mathbf{q})} b^\dagger_{\mathbf{k''}\gamma} \sigma^d_{\gamma\delta} b_{\mathbf{k'''}\delta} e^{i\mathbf{r_j}(\mathbf{k''} - \mathbf{k'''} - \mathbf{q})} \rangle \tag{4.16a}$$

$$= \frac{1}{4N} \sum_{\mathbf{k},\mathbf{k''}} \langle b^\dagger_{\mathbf{k}\alpha} \sigma^c_{\alpha\beta} b_{(\mathbf{k}+\mathbf{q})\beta} b^\dagger_{\mathbf{k''}\gamma} \sigma^d_{\gamma\delta} b_{(\mathbf{k''}-\mathbf{q})\delta} \rangle. \tag{4.16b}$$

Using Bogoliubov transformation matrix $P_{\mathbf{k}}$, we express the bosonic operators $b_{\mathbf{k}}$ in terms of new bosonic operators $\gamma_{\mathbf{k}}$ and $\gamma^{\dagger}_{-\mathbf{k}}$. Since $\gamma_{\mathbf{k}}$ annihilate the vacuum, we can evaluate the expression using Wick's contractions, which is equivalent to performing normal ordering and collecting the "constant" terms.

$$\begin{aligned} S^{cd}(\mathbf{q}) = \frac{1}{4N}\sum_{\mathbf{k},\mathbf{k''}} \langle ((P_{\mathbf{k}})^{*}_{\alpha 3}\gamma_{-\mathbf{k},1} + (P_{\mathbf{k}})^{*}_{\alpha 4}\gamma_{-\mathbf{k},2})\sigma^{c}_{\alpha\beta} \\ ((P_{\mathbf{k+q}})_{\beta 1}\gamma_{\mathbf{k+q},1} + (P_{\mathbf{k+q}})_{\beta 2}\gamma_{\mathbf{k+q},2} + (P_{\mathbf{k+q}})_{\beta 3}\gamma^{\dagger}_{-(\mathbf{k+q})} + (P_{\mathbf{k+q}})_{\beta 4}\gamma^{\dagger}_{-(\mathbf{k+q}),2}) \\ ((P_{\mathbf{k''}})^{*}_{\gamma 1}\gamma^{\dagger}_{\mathbf{k''},1} + (P_{\mathbf{k''}})^{*}_{\gamma 2}\gamma^{\dagger}_{\mathbf{k''},2} + (P_{\mathbf{k''}})^{*}_{\gamma 3}\gamma_{-\mathbf{k''},1} + (P_{\mathbf{k''}})^{*}_{\gamma 4}\gamma_{-\mathbf{k''},2})\sigma^{d}_{\gamma\delta} \\ ((P_{\mathbf{k''-q}})_{\delta 3}\gamma^{\dagger}_{(-\mathbf{k''}+\mathbf{q}),1} + (P_{\mathbf{k''-q}})_{\delta 4}\gamma^{\dagger}_{(-\mathbf{k''}+\mathbf{q}),2})\rangle. \end{aligned} \tag{4.17}$$

We obtain contributions $\delta_{-\mathbf{k},\mathbf{k''}}$, $\delta_{\mathbf{k''},\mathbf{k+q}}$ and $\delta_{\mathbf{q},0}$:

$$\begin{aligned} S^{cd}(\mathbf{q}) = \frac{1}{4N}\sum_{\mathbf{k}} \Big(\langle b^{\dagger}_{\mathbf{k}\alpha}\sigma^{c}_{\alpha\beta}b_{(\mathbf{k+q})\beta}b^{\dagger}_{-\mathbf{k}\gamma}\sigma^{d}_{\gamma\delta}b_{-(\mathbf{k+q})\delta}\rangle + \langle b^{\dagger}_{\mathbf{k}\alpha}\sigma^{c}_{\alpha\beta}b_{(\mathbf{k+q})\beta}b^{\dagger}_{\mathbf{k+q}\gamma}\sigma^{d}_{\gamma\delta}b_{(\mathbf{k})\delta}\rangle \Big) \\ + L^{cd}\delta_{\mathbf{q},0}. \end{aligned} \tag{4.18}$$

The term $L^{cd}\ \delta_{\mathbf{q},0}$ is proportional to $< S^{c} >< S^{d} >$ and is thus zero, when the state is in spin liquid phase. Evaluation of Wick's contractions leads to many terms. To compute them, we made use of the excellent Mathematica package for symbolic calculations with second-quantization-operator expressions SNEG [25]. The resulting expressions have the form:

$$S^{cd}(\mathbf{q}) = \frac{1}{\mathrm{Vol}_k}\int \mathrm{d}^2k f^{cd}(P_{\mathbf{k}}, P_{\mathbf{k+q}}), \tag{4.19}$$

where $f^{cd}(P_{\mathbf{k}}, P_{\mathbf{k+q}})$ is a complicated function of around 50 terms consisting of the elements of the transformation matrices $P_{\mathbf{k}}$ and $P_{\mathbf{k+q}}$. An expression for $f^{xx}(P_{\mathbf{k}}, P_{\mathbf{k+q}})$ is given in the appendix A.2.

Chapter 5

Results and Discussion

It this chapter we present the results of our approach. First, we show solutions of the self-consistency equations, i.e. the saddle points of E_{MF}. We argue that they correspond to three distinct phases. Then we characterise these three phases by looking at the spinon dispersion relations and the static spin structure factors. Furthermore, we look at the non-diagonal parts of the spin structure factors $S^{cd}(\mathbf{q})$ defined before. Lastly, we present the results of an analysis of the classical limit.

5.1 Self-consistent Mean-field Parameters

Self-consistent mean-field parameters are obtained by searching for the saddle points of E_{MF} as explained in Chapter 4. To make sure our algorithm for the determination of the saddle points works as expected, we test it at the Heisenberg ($J_K = 0$) point. The resulting energy agrees with the value provided in Subir Sachdev's paper [8] [1].

The resulting values of A, t and B at the saddle points are shown in Figure 5.1. We identify three phases. In SL1, the fields A and B are nonzero, SL2 has all three parameters nonzero, SL3 only has the field t different from zero. The resulting phase diagram is shown in Figure 5.2.

We notice that the region of SL2 grows with the spin size S. If we increase S further from 0.2, at least for some values of ψ the spinon gap closes and a Bose-Einstein condensate is formed, indicating a magnetically ordered state.

For further characterization, we will focus on six saddle points at $S = 0.14$ shown in Table 5.1.

Phase	ψ	A	t	B	λ	E_{MF}
SL1	0	0.181	0	-0.0528	0.4025	-0.0901
SL2	0.6	0.176	0.0389	-0.0476	0.303	-0.0701
SL2	0.8	0.132	0.117	-0.023	0.281	-0.0635
SL2	0.85	0.109	0.135	-0.0147	0.276	-0.0634
SL2	0.9	0.0687	0.154	-0.0055	0.272	-0.0645
SL3	$\frac{\pi}{2}$	0	0.165	0	0.338	-0.082

Table 5.1: Six saddle points at S=0.14 used for further discussion.

[1] Sachdev used the decoupling $\mathbf{S_i} \cdot \mathbf{S_j} = S^2 - 2 : A^\dagger_{ij} A_{ij} :$ with only A fields, so for this test we needed to change $J_H \to 2J_H$, add constant term $J_H S^2$ and set B fields to zero.

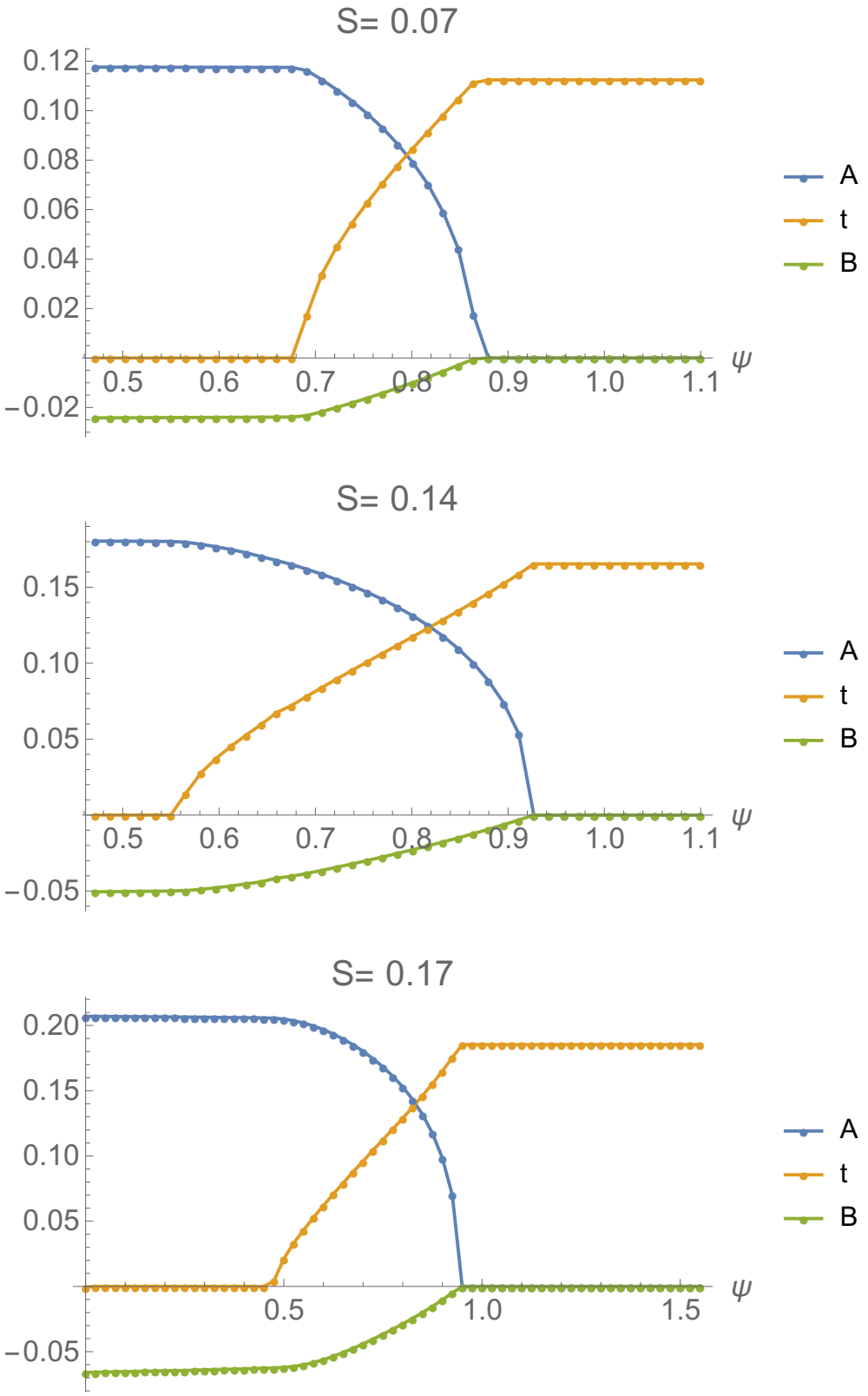

Figure 5.1: Values of A,t and B for different values of $\psi = \arctan(J_K/J_H)$ at three values of spin size S. In all three cases we have a finite excitation gap and thus a $\mathbb{Z}_2$ spin liquid phase.

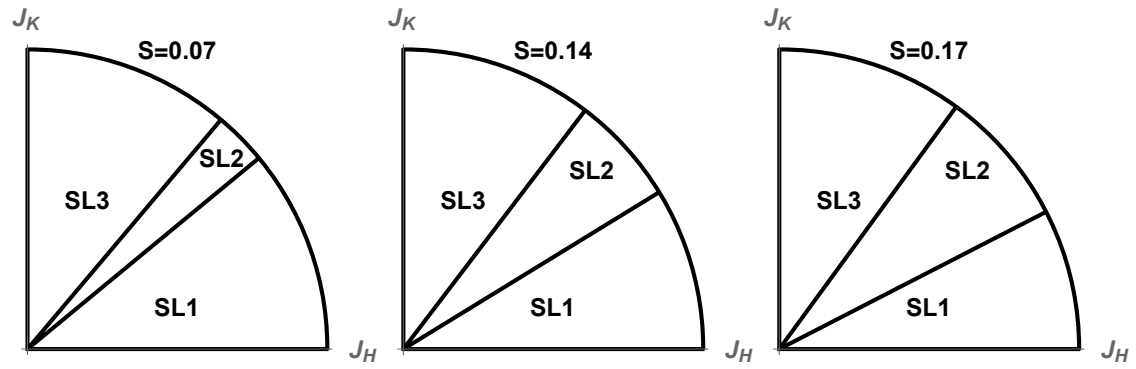

Figure 5.2: Phase diagrams for three values of S.

5.2 Dispersion

The spinon dispersion is not a gauge invariant quantity, nevertheless it is an interesting object to look at. When the value of S is increased, the excitation gap closes at some values of $\mathbf{q}$ in the Brillouin zone. Further increasing the value of S, we develop Bose Einstein condensate at these points, which then determine the Bragg peaks of static spin structure factor.

The typical lower branch of dispersions are shown in Figure 5.3. The minima of the dispersion in SL1 are at the K points in the corners of the first Brillouin zone, which is consistent with previous results [8], resulting in 120-degree order for larger values of S. The minima in SL3 occur at the M points in the middle of the edges of the first Brillouin zone and at Γ point at 0.

In a region of SL2 close to SL1 the minima stay in the corners of the first Brillouin zone. Then, by increasing ψ, the minima start to move along the edge of the first Brillouin zone and are thus located at incommensurate momenta. For some values of ψ and S, the global minima jump to zero momentum, which we believe to be an artefact of the mean-field approximation. It would imply a spinon condensate at Γ point that correspond to ferromagnetic state, which is not expected for antiferromagnetic couplings J_H and J_K. We think that B fields are overestimated, decreasing the value of B fields by a few percent shifts the absolute minima back to incommensurate momenta.

All these situations are very close in energy and parameters, thus the mean-field analysis is probably not enough to always accurately determine the position of the minima in SL2. Indeed, we will later show that dispersion minima at incommensurate momenta are in accordance with the expected magnetic order in the classical limit.

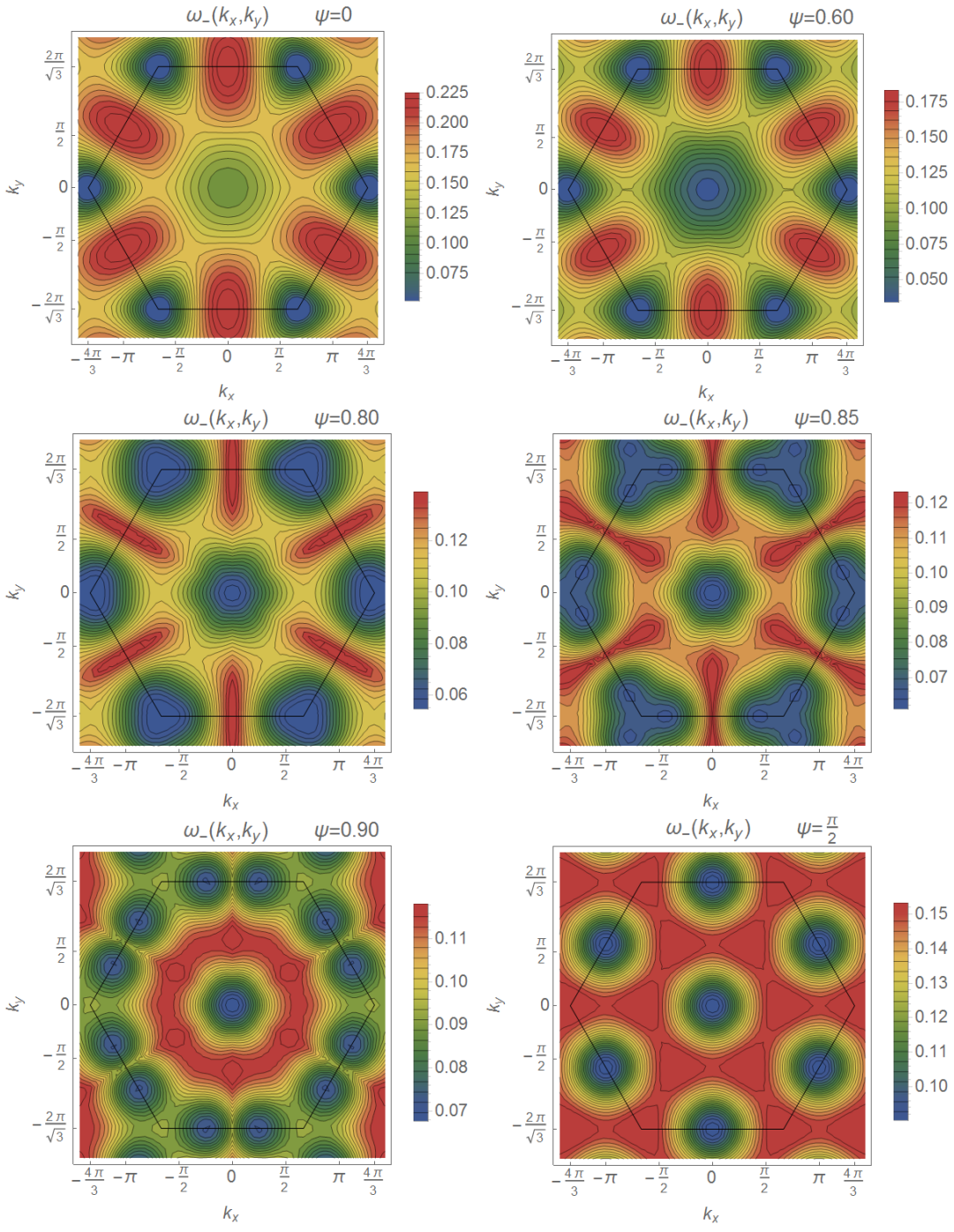

Figure 5.3: Lower branch of the spinon dispersion $\omega_-(\mathbf{k})$ for the six points shown in Table 5.1. The black hexagon marks the boundary of the first Brillouin zone. Note that the local minima shift from the corner of the first Brillouin zone (K point) in the SL1, through incommensurate momenta and Γ point ($\mathbf{q} = 0$) in SL2 to the middle of the edges of the first Brillouin zone and zero (M and Γ points). The global minimum in SL2 can be either at K point, Γ point or incommensurate momenta depending on ψ and S (see main text for a discussion).

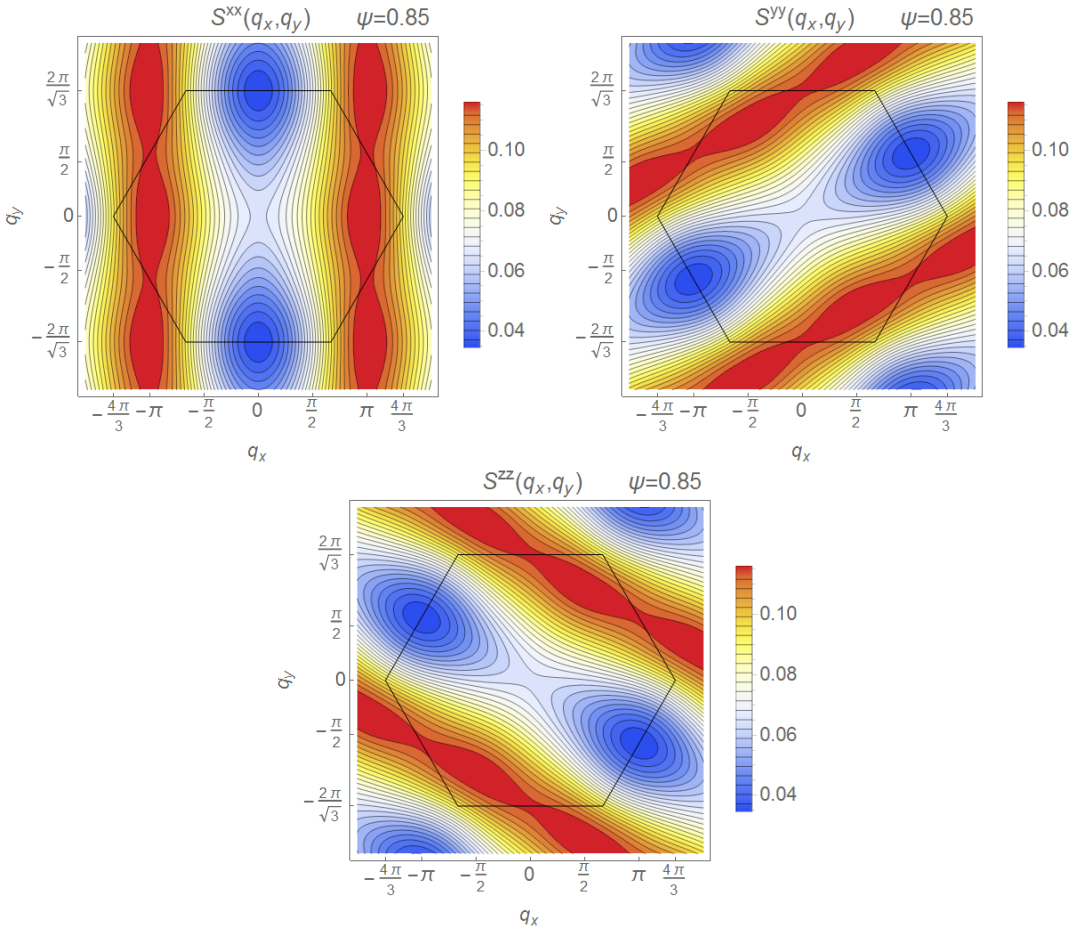

Figure 5.4: Diagonal elements $S^{aa}(\mathbf{q})$ at $\psi = 0.85$. We see that diagonal elements $S^{yy}(\mathbf{q})$ and $S^{zz}(\mathbf{q})$ are simply $S^{xx}(\mathbf{q})$ rotated by $\pm\frac{\pi}{3}$.

5.3 Static Spin Structure Factor

The static spin structure factor can be measured directly in neutron scattering experiments. In the spin liquid ground state neutron excites two (fractionalized) spinon excitations, and the structure factor is continuous. On the other hand, neutron excites only one magnon (spin wave) in the spin ordered phase, so we have sharp Bragg peaks in the spin structure factor.

We have derived how to compute the static spin structure factor in the section 4.4. In Figure 5.5 we show the results for the xx-component $S^{xx}(\mathbf{q})$ of the static spin structure factor for the six different saddle points listed in Table 5.1. Notice that the maxima change the position to incommensurate momenta in the SL2 phase. The other diagonal elements $S^{yy}(\mathbf{q})$ and $S^{zz}(\mathbf{q})$ are simply $S^{xx}(\mathbf{q})$ rotated by $\pm\frac{\pi}{3}$ as shown in Figure 5.4.

The total static spin structure factor can be computed from the diagonal elements by

$$S(\mathbf{q}) = S^{xx}(\mathbf{q}) + S^{yy}(\mathbf{q}) + S^{zz}(\mathbf{q}), \tag{5.1}$$

and is shown in Figure 5.6. Here, the maxima stay at commensurate momenta in all phases, since the maxima of the diagonal elements $S^{aa}(\mathbf{q})$ are broad.

We also note that even though the total magnetization $\langle \sum_i \mathbf{S}_i \rangle = 0$ in the spin liquid ground state per construction, the variance of the total spin $\langle (\sum_i \mathbf{S}_i)^2 \rangle$ is

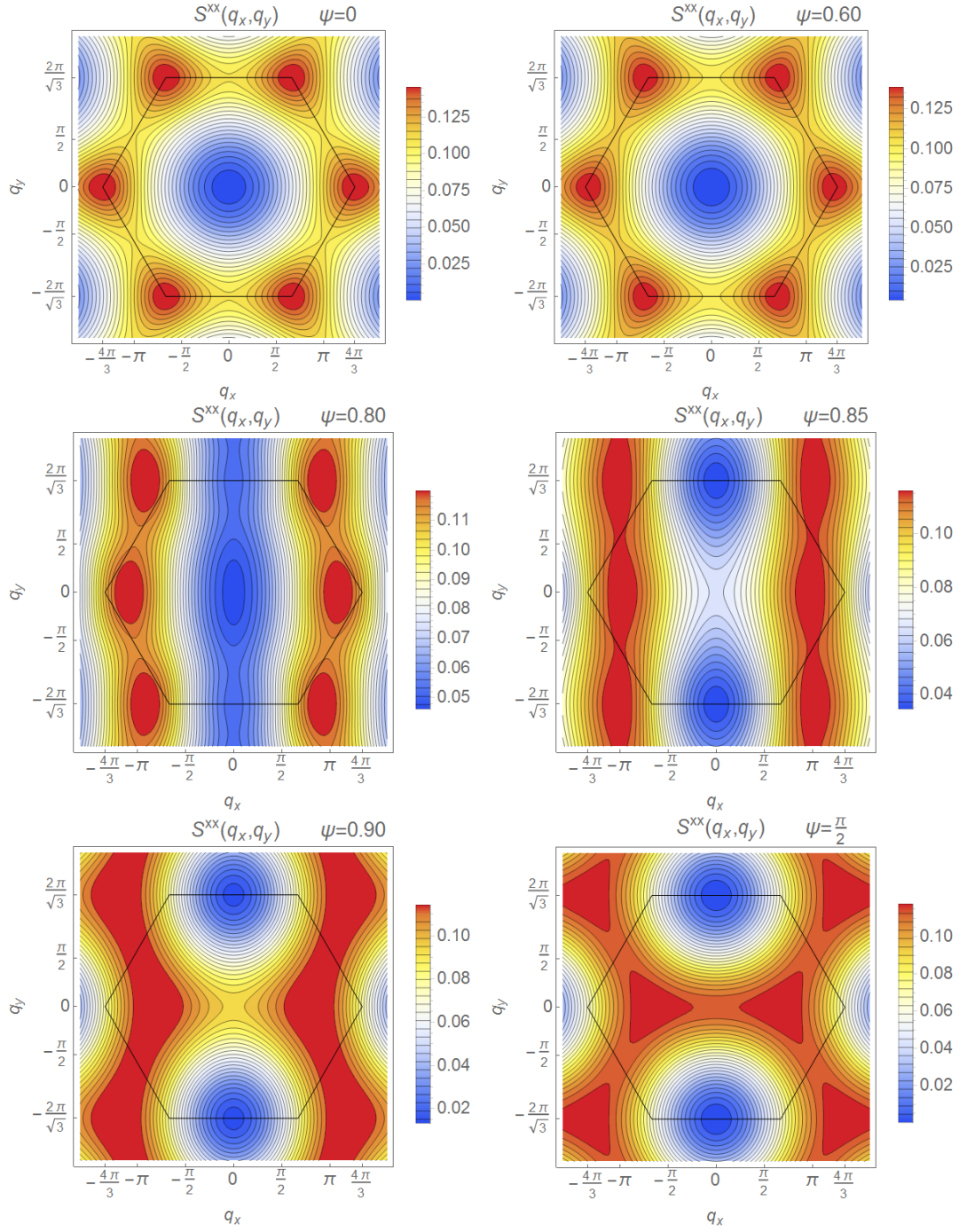

Figure 5.5: $S^{xx}(\mathbf{q})$ for the six points shown in Table 5.1. We see that the maxima change position in SL2 to incommensurate momenta.

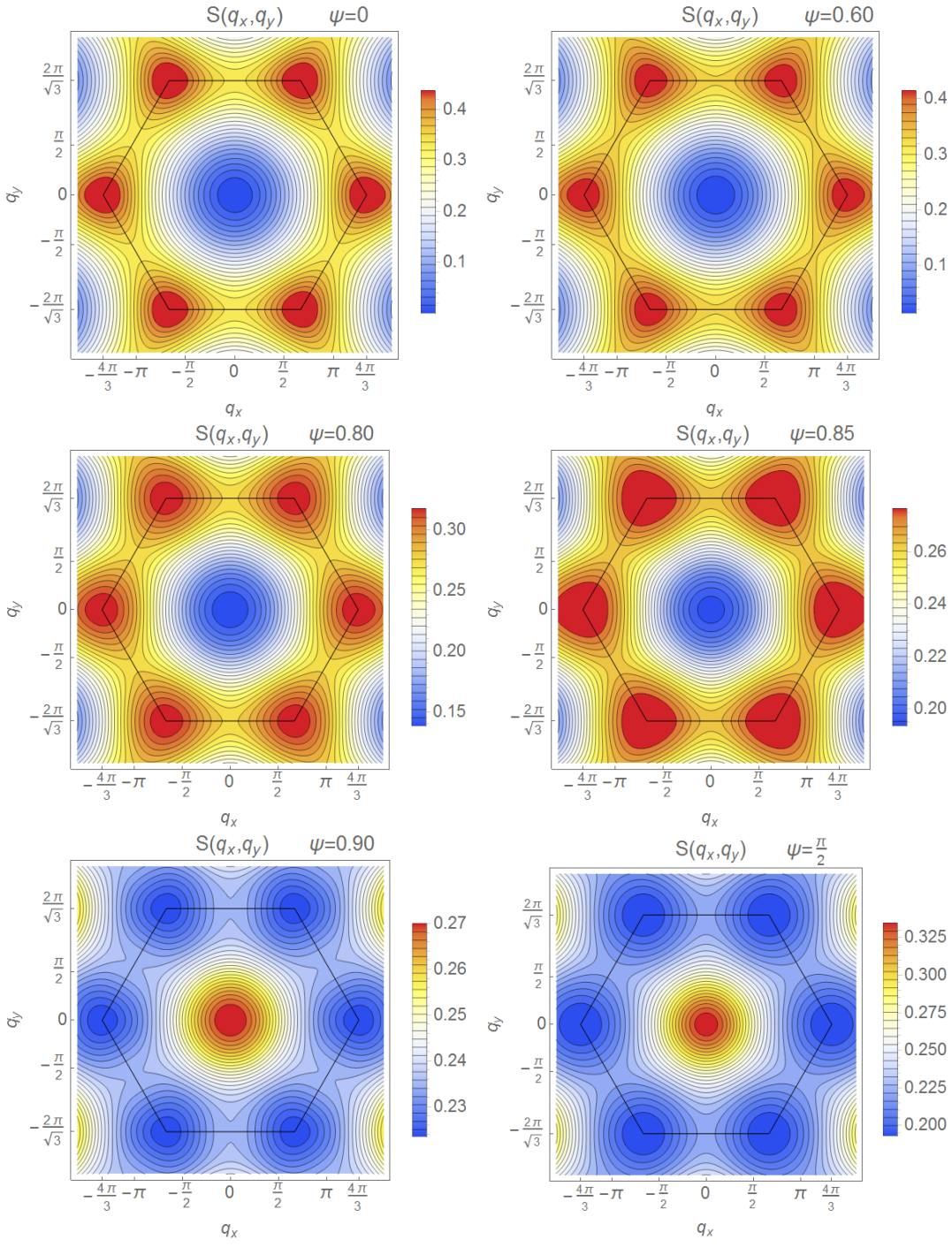

Figure 5.6: The static spin structure factor $S(\mathbf{q})$ for the six points shown in Table 5.1. The peaks of $S^{aa}(\mathbf{q})$ are so broad, that the maxima of $S(\mathbf{q})$ stay at the commensurate momenta.

non-zero in the SL2 and SL3 phase. We see that this indeed holds by observing non-zero structure factor at zero momenta in SL2 and SL3 phases. This is because the ground state is not a total spin singlet, which is in accordance with non-zero expectation value of the triplet fields $\hat{t}_\gamma$.

Off-diagonal Elements

The striking difference between the SL2 phase and the other two phases is that the phases SL1 and SL3 have **vanishing** off-diagonal elements $S^{ab}(\mathbf{q})$ defined in equation 4.15, but they are **non-zero** in SL2.

These non-zero off-diagonal elements indicate correlations of different spin components. Even though the matrix $S^{ab}(\mathbf{q})$ can be diagonalized for a specific momentum $\mathbf{q}$, it can not be diagonalized for all momenta at once using the same transformation matrix. The real and imaginary parts of the off-diagonal elements $S^{ab}(\mathbf{q})$ for the fourth point ($\psi = 0.85$) in Table 5.1 are shown in Figure 5.7.

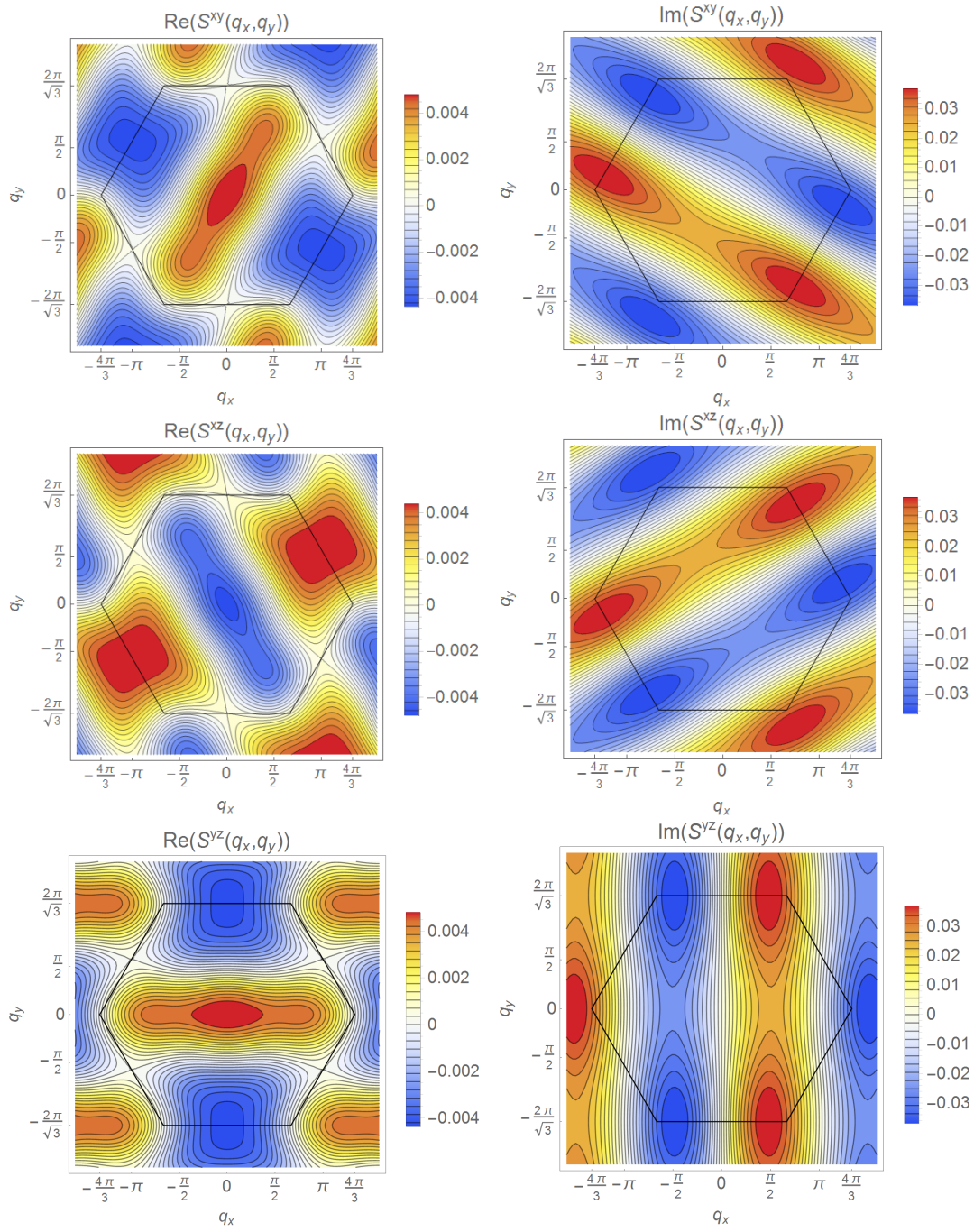

Figure 5.7: Real and imaginary part of off-diagonal elements $S^{ab}(\mathbf{q})$ in SL2 computed for the fourth point ($\psi = 0.85$) in Table 5.1. Note that these non-zero off-diagonal values of $S^{ab}(\mathbf{q})$ imply correlations of different spin components in the SL2 phase. By contrast, the off-diagonal elements vanish in the SL1 and SL3 phases. Furthermore, we see that the maxima of the imaginary part are at incommensurate momenta.

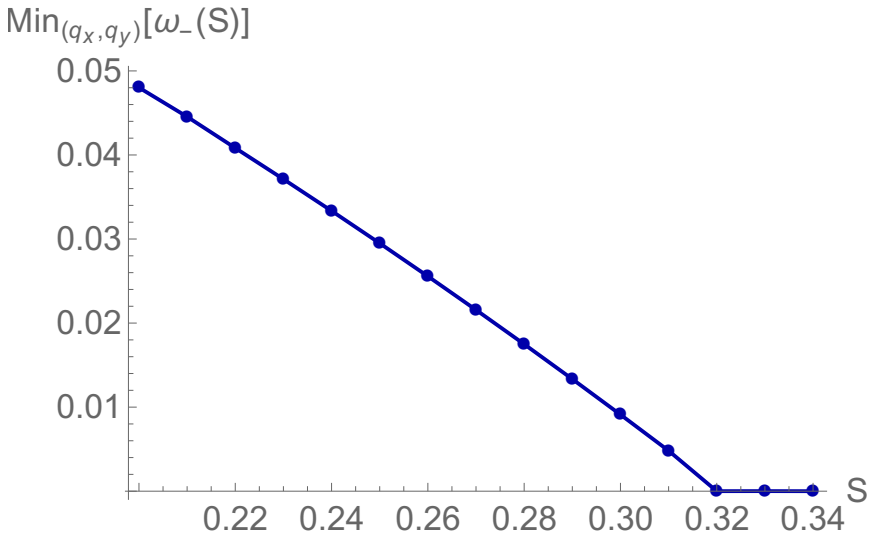

Figure 5.8: Minima of dispersion with respect to S at $\psi = 0.9$. We see that the gap closes at $S \approx 0.32$.

5.4 Condensation and Classical Limit

In this section we will investigate the condensed state. When the parameter S increases, the minima of the excitation gap closes at some S_c as is shown in Figure 5.8.

Further increasing S adds bosons in the zero modes and Bose-Einstein condensate forms, i.e. we get a nonzero expectation value of $\langle b \rangle$. This means that we get a nonzero ordered magnetic moment. The size of the ordered magnetic moment (density of Bose-Einstein condensate) is determined by S through the saddle point conditions.

We know that condensation happens at zero modes momenta $\mathbf{k_{ci}}$, where i runs over all nonequivalent zero modes in the first Brillouin zone. This in turn determines the possible positions of Bragg peaks as the differences of zero mode momenta $\mathbf{k_{ci}} - \mathbf{k_{cj}}$ as is schematically shown in Figure 5.9 for the SL2 phase. The eigenvectors of $\tau^z H_{\mathbf{k}}$ in the Bogoliubov transformation matrix $P_{\mathbf{k_c}}$ contain additional information about the structure of the ordered phase.

5.4.1 Classical Limit in SL1 phase

The SL1 phase is the phase appearing in the Heisenberg model on the triangular lattice. The classical limit has been derieved by Sachdev [8] and by Fa Wang and A. Vishwanath [9].

Condensation happens at the corners (K points) of the first Brillouin zone. There are only two distinctive points $\mathbf{k_c} = (4\pi/3, 0)$ and $-\mathbf{k_c}$, the rest of the corners can be reached by reciprocal vectors $\mathbf{G_1}$ and $\mathbf{G_2}$ shown in Figure 4.1. The structure of the condensate is determined by the eigenvectors of the matrix $\tau^z H_{\mathbf{k}}$, which are the columns of the Bogoliubov transformation matrix $P_{\mathbf{k_c}}$:

$$\begin{aligned} \psi_1(\mathbf{k_c}) &= (i, 0, 0, 1)^T, \\ \psi_2(\mathbf{k_c}) &= (0, -i, 1, 0)^T. \end{aligned} \tag{5.2}$$

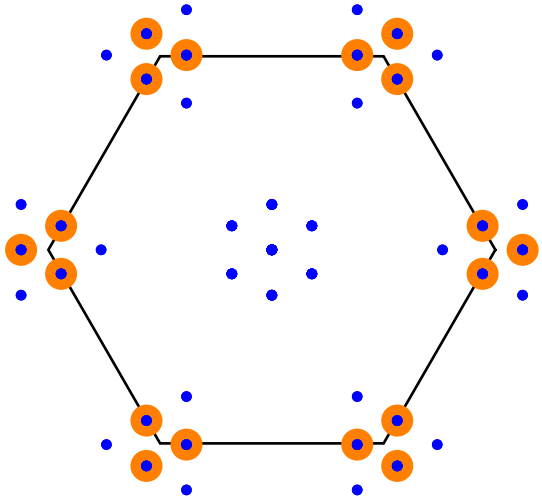

Figure 5.9: Schematic picture showing how in the SL2 phase the positions of zero modes (orange) at $\mathbf{k_{ci}}$ determine the possible positions of Bragg peaks of the static spin structure factor (blue) as the differences $\mathbf{k_{ci}} - \mathbf{k_{cj}}$.

The condensate has thus the form:

$$\langle \begin{pmatrix} b_{\mathbf{k_c}\uparrow} \\ b_{\mathbf{k_c}\downarrow} \\ b^\dagger_{-\mathbf{k_c}\uparrow} \\ b^\dagger_{-\mathbf{k_c}\downarrow} \end{pmatrix} \rangle = s_1\psi_1(\mathbf{k_c}) + s_2\psi_2(\mathbf{k_c}) = \begin{pmatrix} is_1 \\ -is_2 \\ s_2 \\ s_1 \end{pmatrix} \tag{5.3}$$

with only $|s_1|^2 + |s_2|^2$ determined by the size of spin S. The spin expectation value in real space has the following form:

$$x \equiv \langle \begin{pmatrix} b_{\mathbf{r}\uparrow} \\ b_{\mathbf{r}\downarrow} \end{pmatrix} \rangle = \begin{pmatrix} is_1 e^{i\mathbf{k_c r}} + s_2^* e^{-i\mathbf{k_c r}} \\ -is_2 e^{i\mathbf{k_c r}} + s_1^* e^{-i\mathbf{k_c r}} \end{pmatrix} = \begin{pmatrix} ic_1 e^{i\mathbf{k_c r}} - ic_2 e^{-i\mathbf{k_c r}} \\ c_2^* e^{i\mathbf{k_c r}} + c_1^* e^{-i\mathbf{k_c r}} \end{pmatrix} \tag{5.4}$$

where we rewrote the constants as $c_1 = s_1$ and $c_2 = is_2^*$ to match the expression on page 9 in the reference [9].

The ordered magnetic moment can easily be calculated from x as $\mathbf{S}(\mathbf{r}) = \frac{1}{2}x^\dagger \sigma x$. When plotted, we recognise the 120-degree order shown in Figure 2.4. The freedom of choice of c_1 and c_2 is just a consequence of the global SU(2) symmetry, i.e. changing them rotates the plane in which the spins order.

5.4.2 Classical Limit in SL3 phase

The treatment of classical limit in SL3 phase is quite a bit more cumbersome, because now we have four nonequivalent zero modes at three nonequivalent M points and at Γ point as shown in Figure 5.10. Furthermore, the Hamiltonian is not SU(2) symmetric. The zero modes occur at the following nonequivalent momenta:

$$\begin{aligned} \mathbf{k_{c0}} &= (0,0) & \mathbf{k_{c1}} &= (0, \frac{2\pi}{\sqrt{3}}) \\ \mathbf{k_{c2}} &= (\pi, \frac{\pi}{\sqrt{3}}) & \mathbf{k_{c3}} &= (\pi, -\frac{\pi}{\sqrt{3}}). \end{aligned} \tag{5.5}$$

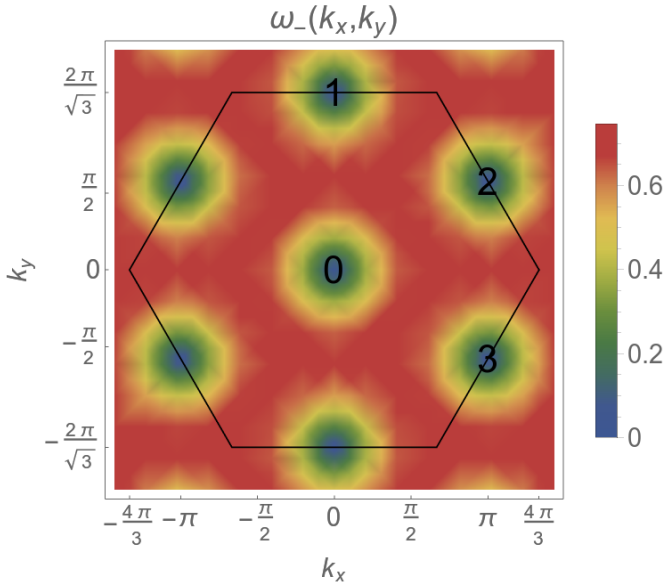

Figure 5.10: Dispersion in SL3 at the condensation point. The distinct eigenmodes are labeled by 0 to 3.

There are two eigenvectors of $\tau^z H_{\mathbf{k_{ci}}}$ for every zero mode:

$$\psi_{01} = \left(\frac{1-i}{\sqrt{6}}, \frac{i}{\sqrt{6}}, \frac{1}{\sqrt{2}}, 0\right)^T, \tag{5.6a}$$

$$\psi_{02} = \left(\frac{i}{\sqrt{6}}, \frac{1+i}{\sqrt{6}}, 0, \frac{1}{\sqrt{2}}\right)^T, \tag{5.6b}$$

$$\psi_{11} = \left(\frac{-1-i}{\sqrt{6}}, \frac{-i}{\sqrt{6}}, \frac{1}{\sqrt{2}}, 0\right)^T, \tag{5.6c}$$

$$\psi_{12} = \left(\frac{-i}{\sqrt{6}}, \frac{-1+i}{\sqrt{6}}, 0, \frac{1}{\sqrt{2}}\right)^T, \tag{5.6d}$$

$$\psi_{21} = \left(\frac{1+i}{\sqrt{6}}, \frac{-i}{\sqrt{6}}, \frac{1}{\sqrt{2}}, 0\right)^T, \tag{5.6e}$$

$$\psi_{22} = \left(\frac{-i}{\sqrt{6}}, \frac{1-i}{\sqrt{6}}, 0, \frac{1}{\sqrt{2}}\right)^T, \tag{5.6f}$$

$$\psi_{31} = \left(\frac{-1+i}{\sqrt{6}}, \frac{i}{\sqrt{6}}, \frac{1}{\sqrt{2}}, 0\right)^T, \tag{5.6g}$$

$$\psi_{32} = \left(\frac{i}{\sqrt{6}}, \frac{-1-i}{\sqrt{6}}, 0, \frac{1}{\sqrt{2}}\right)^T. \tag{5.6h}$$

Accordingly, the condensate has the form:

$$\left\langle \begin{pmatrix} b_{\mathbf{k}\uparrow} \\ b_{\mathbf{k}\downarrow} \\ b^\dagger_{-\mathbf{k}\uparrow} \\ b^\dagger_{-\mathbf{k}\downarrow} \end{pmatrix} \right\rangle = \sum_{i=0}^{3} \left(c_{i1}\psi_{i1} + c_{i2}\psi_{i2}\right) \delta_{\mathbf{k},\mathbf{k_{ci}}} \tag{5.7}$$

In contrast to the SL1 case, we now have 8 complex constants c_{ij} determining the spin order. In SL3 case the points at $\mathbf{k_{ci}}$ and $-\mathbf{k_{ci}}$ are equivalent as they are

connected by the linear combination of the lattice reciprocal vectors $\mathbf{G_1}$ and $\mathbf{G_2}$. For the description to be self-consistent, $\langle b_{\mathbf{k_{ci}}\alpha}\rangle = \langle b_{-\mathbf{k_{ci}}\alpha}\rangle$ must hold, which gives 4 nonequivalent equations:

$$c_{i1}^*(\psi_{i1})_3 + c_{i2}^*(\psi_{i2})_3 = c_{i1}(\psi_{i1})_1 + c_{i2}(\psi_{i2})_1, \tag{5.8}$$

where i goes from 0 to 3.

After taking these equations into account, we are still left with four complex parameters, that need to be fixed to obtain the spin order parameter. To fix them, we would need to go beyond mean-field description in order to take the interactions between zero modes into account.

We avoid this problem by making some reasonable assumptions about the condensate. Firstly, we demand constant density of condensed bosons at each lattice site, meaning that the ordered spin length is the same at each lattice site. Since the order is commensurate, we have only four distinctive sites and this can be done. This assumption definitely holds in the classical limit $S \to \infty$.

Secondly, we demand zero total magnetization. Thirdly, we demand that either all four or two modes have the same occupancy. The total occupancy is determined by the spin size S through $\sum_{i=0}^{3}(|c_{i1}|^2 + |c_{i2}|^2) = 2S$. We have numerically solved for these constraints, the result is shown in Figure 5.11. Because of D_{2h} degeneracy in the spin space, similar states can also be obtained that are ordered in different directions. The ordered spin momentum can be written as:

$$\mathbf{S}(n,m) = \frac{1}{\sqrt{2}}\left((-1)^{n+m}, 0, (-1)^n\right)^T \tag{5.9a}$$

$$\mathbf{S}(n,m) = \frac{1}{\sqrt{2}}\left((-1)^{n+m}, (-1)^{n+m}, 0\right)^T, \tag{5.9b}$$

where in the first expression all four modes have the same condensate density, whereas in the second expression only two modes 1 and 2 or 0 and 3 are condensed with the same density and the other two are equal to zero. Here, we labelled sites on the triangular lattice by the integers n and m via $\mathbf{r} = n\mathbf{a_x} + m\mathbf{a_y} = (n,m)$. Note that both solutions belong to SO(2) degenerate ground state manifold of the classical Kitaev model on the triangular lattice with the energy $E_0 = -NJ_K$.

5.4.3 Classical Limit in SL2 phase

Lastly, we discuss the classical limit in SL2 phase. Assuming the condensation happens at six distinct incommensurate momenta, this determines the possible positions of Bragg peaks (see Figure 5.9). This is in accordance with the classical $\mathbb{Z}_2$ vortex phase, which is the ground state of the classical Heisenberg-Kitaev model for $J_H > 0$ and $J_K > 0$ [7, 6].

Because the condensation happens at six distinctive points, there are too many parameters and not enough constraints to determine the structure of the condensate and magnetic order parameter within mean-field theory. The interactions between zero modes become important.

However, because our ansatz is real and thus time reversal symmetric, the classical limit (if it exists) corresponds to coplanar state [23], which is different from non-coplanar $\mathbb{Z}_2$ vortex phase. This is apparent by looking at the scalar spin chirality

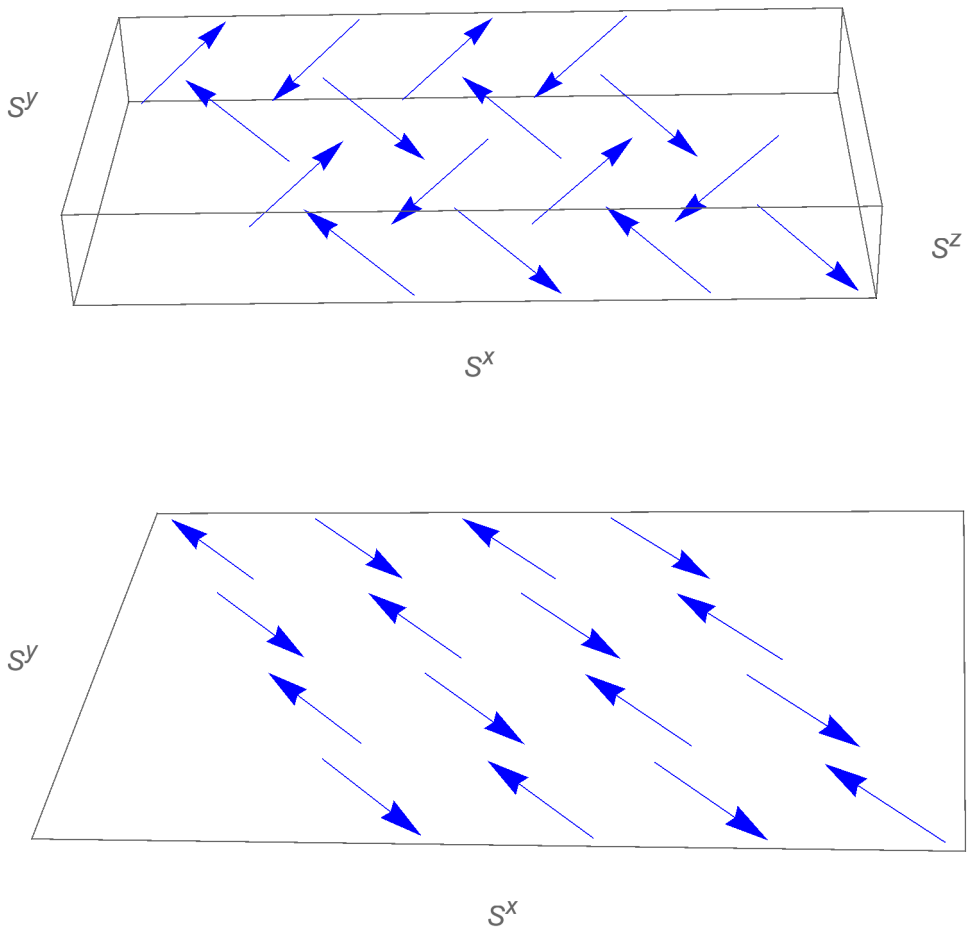

Figure 5.11: The ordered spin configurations from SL3 phase. Top: we condensed all four modes with the same densities. Bottom: Condensed modes 1 and 2 with the same density. For better visibility we have plotted S^γ along the γ' direction, and not along the γ direction (γ =x,y,z) shown in Figure 2.6.

defined for spins on an elementary triangle

$$\chi_{ijk} = \mathbf{S}_i \cdot (\mathbf{S}_j \times \mathbf{S}_k) \sim \mathrm{Im}(\hat{B}_{ij}\hat{B}_{jk}\hat{B}_{ki}) = 0. \tag{5.10}$$

All in all, the classical limit in SL2 has proven to be inaccessible using only mean-field approach.

5.5 Discussion

We have shown that we can use the Schwinger-boson mean-field treatment to study the Heisenberg-Kitaev model on the triangular lattice. Using a simple symmetric ansatz we get a phase diagram consisting of three spin liquid phases for small spin size S. Condensation occurs at $S \approx 0.3$, meaning that we expect the physical spin one-half system to have some ordered spin signature, if the quantum effects are not underestimated. But proximity to spin liquid still plays an important role.

The SL1 phase occurs close to the Heisenberg point and it has the 120-degree order as its classical limit. This agrees with previous results of the Heisenberg model on the triangular lattice.

Increasing the antiferromagnetic Kitaev coupling J_K leads to the SL2 phase, which has interesting properties. The minima of the dispersion relation can change the position to incommensurate momenta. This could imply that the classical limit of SL2 leads to a $\mathbb{Z}_2$ vortex crystal phase, but we were not able to show this using our simple methods. The off-diagonal elements of S^{ab} were non-zero in SL2, in contrast to SL1 and SL3. Furthermore, diagonal and off-diagonal elements have their maxima shifted away from the corner points in the first Brillouin zone to incommensurate momenta.

The SL3 phase has the minima of the dispersion relation at M and Γ points. We have shown that in the classical limit (under reasonable assumptions) we recover the classical ground states of the Kitaev model on the triangular lattice. The S^{ab} is again diagonal, but with different values on the diagonal.

Ansates with $p_1 = 1$ have a doubled unit cell resulting in increasing the complexity of the problem, since $H_{\mathbf{k}}$ is now 8×8 matrix. But, we have quickly looked at other $p_1 = 0$ ansatzes. The $k = 1$, $\phi_B = 0$ and $\phi_t = 0$ ansatz showed only two spin liquids, separated by a first order phase transition. Interesting was an ansatz with $k = 0$, $\phi_t = 0$ and ϕ_B determined by a saddle point, since this ansatz can change chirality continuously $\chi_{ijk} \sim \mathrm{Im}(\hat{B}_{ij}\hat{B}_{jk}\hat{B}_{ki}) = |B|\sin(3\phi_B)$. But the saddle point condition set $\phi_B = 0$ or $|B| = 0$ depending on if we looked at maximum or minimum of the free energy with respect to ϕ_B.

Chapter 6

Conclusion and Outlook

We investigated the Heisenberg-Kitaev model on the triangular lattice using the Schwinger-Boson mean-field approach for antiferromagnetic Heisenberg and Kitaev couplings focusing on the potential quantum disordered $\mathbb{Z}_2$ spin liquid ground states.

After reviewing the most important theoretical background, we introduced the model and performed the mean-field decoupling. Then we spent quite some time describing a systematic way of obtaining the mean-field ansatzes with the use of the projective symmetry (PSG) group approach. We extend it to non-SU(2) symmetric case of Heisenberg-Kitaev model and obtained weakly symmetric ansatzes.

In the following, we focused on the only totally symmetric ansatz. We preformed a Bogoliubov transformation to diagonalize the problem and then searched for the saddle points of free energy to determine the mean-field parameters self-consistently. Furthermore, we derived the one spinon dispersion and static spin structure factor.

In chapter 5, we presented the results of the simplest ansatz. We noticed three spin liquid phases separated by a continuous quantum phase transition, which we characterised. The SL1 phase was shown to be the spin liquid phase discussed by previous works for the Heisenberg model on the triangular lattice. The SL2 phase showed interesting dispersion with the minima at incommensurate momenta. It was shown that the phase exhibits correlations of different spin components in contrast to SL1 and SL3. Moreover, the maxima of the elements of static spin structure tensor S^{ab} are shifted to incommensurate momenta. Close to the Kitaev point, we found a SL3 spin liquid phase, for which we calculated the dispersion and static spin structure factor. Furthermore, we investigated the classical limit of this phase and showed that we recover classical ground states.

It appears that we have discovered a continuous phase transition between three symmetry enriched topological (SET) phases, where the gap stays finite. In the future, it would be interesting to further investigate this interesting fact. Also, focusing on other ansatzes obtained from our PSG analysis and comparing them with our results would be also interesting. Calculating the dynamical structure factor would give further characterization of the phases and it could be measured by neutron scattering experiments and compared with theoretical predictions. Another interesting possibility would be to try to go beyond the mean-field approximation and introduce coupling to the gauge fields. A study focusing on the excitations would shed light on the topological nature of the resulting phase.

Bibliography

[1] Leon Balents. "Spin liquids in frustrated magnets". In: *Nature* 464.7286 (2010), pp. 199–208.

[2] Subir Sachdev. "Quantum magnetism and criticality". In: *Nature Physics* 4.3 (2008), pp. 173–185.

[3] Lucile Savary and Leon Balents. "Quantum Spin Liquids". In: *arXiv preprint arXiv:1601.03742* (2016).

[4] Xiao-Gang Wen. "Quantum orders and symmetric spin liquids". In: *Phys. Rev. B* 65 (16 Apr. 2002), p. 165113.

[5] Itamar Kimchi and Ashvin Vishwanath. "Kitaev-Heisenberg models for iridates on the triangular, hyperkagome, kagome, fcc, and pyrochlore lattices". In: *Phys. Rev. B* 89 (1 Jan. 2014), p. 014414.

[6] Michael Becker, Maria Hermanns, Bela Bauer, Markus Garst, and Simon Trebst. "Spin-orbit physics of $j = \frac{1}{2}$ Mott insulators on the triangular lattice". In: *Phys. Rev. B* 91 (15 Apr. 2015), p. 155135.

[7] Ioannis Rousochatzakis, Ulrich K. Rössler, Jeroen van den Brink, and Maria Daghofer. "Kitaev anisotropy induces mesoscopic $\mathbb{Z}_2$ vortex crystals in frustrated hexagonal antiferromagnets". In: *Phys. Rev. B* 93 (10 Mar. 2016), p. 104417.

[8] Subir Sachdev. "Kagome- and triangular-lattice Heisenberg antiferromagnets: Ordering from quantum fluctuations and quantum-disordered ground states with unconfined bosonic spinons". In: *Phys. Rev. B* 45 (21 June 1992), pp. 12377–12396.

[9] Fa Wang and Ashvin Vishwanath. "Spin-liquid states on the triangular and Kagomé lattices: A projective-symmetry-group analysis of Schwinger boson states". In: *Phys. Rev. B* 74 (17 Nov. 2006), p. 174423.

[10] Gregoire Misguich. *Quantum spin liquids*. 2008. eprint: `arXiv:0809.2257`.

[11] P.W. Anderson. "Resonating valence bonds: A new kind of insulator?" In: *Materials Research Bulletin* 8.2 (1973), pp. 153–160.

[12] Alexei Kitaev. "Anyons in an exactly solved model and beyond". In: *Annals of Physics* 321.1 (2006). January Special Issue, pp. 2–111.

[13] G. Baskaran, Saptarshi Mandal, and R. Shankar. "Exact Results for Spin Dynamics and Fractionalization in the Kitaev Model". In: *Phys. Rev. Lett.* 98 (24 June 2007), p. 247201.

[14] Tusharkanti Dey, A. V. Mahajan, P. Khuntia, M. Baenitz, B. Koteswararao, and F. C. Chou. "Spin-liquid behavior in $J_{\text{eff}} = \frac{1}{2}$ triangular lattice compound $Ba_3IrTi_2O_9$". In: *Phys. Rev. B* 86 (14 Oct. 2012), p. 140405.

[15] Andrei Catuneanu, Jeffrey G. Rau, Heung-Sik Kim, and Hae-Young Kee. "Magnetic orders proximal to the Kitaev limit in frustrated triangular systems: Application to $Ba_3IrTi_2O_9$". In: *Phys. Rev. B* 92 (16 Oct. 2015), p. 165108.

[16] Giniyat Khaliullin and Satoshi Okamoto. "Quantum Behavior of Orbitals in Ferromagnetic Titanates: Novel Orderings and Excitations". In: *Phys. Rev. Lett.* 89 (16 Sept. 2002), p. 167201.

[17] Giniyat Khaliullin. "Orbital order and fluctuations in Mott insulators". In: *Progress of Theoretical Physics Supplement* 160 (2005), pp. 155–202.

[18] Kazuya Shinjo, Shigetoshi Sota, Seiji Yunoki, Keisuke Totsuka, and Takami Tohyama. *Density-matrix renormalization group study of Kitaev-Heisenberg model on the triangular lattice*. 2015. eprint: `arXiv:1512.02334`.

[19] Kai Li, Shun-Li Yu, and Jian-Xin Li. "Global phase diagram, possible chiral spin liquid, and topological superconductivity in the triangular Kitaev–Heisenberg model". In: *New Journal of Physics* 17.4 (2015), p. 043032.

[20] George Jackeli and Adolfo Avella. "Quantum order by disorder in the Kitaev model on a triangular lattice". In: *Phys. Rev. B* 92 (18 Nov. 2015), p. 184416.

[21] N. Read and Subir Sachdev. "Large- N expansion for frustrated quantum antiferromagnets". In: *Phys. Rev. Lett.* 66 (13 Apr. 1991), pp. 1773–1776.

[22] G. Misguich. "Schwinger boson mean-field theory: Numerics for the energy landscape and gauge excitations in two-dimensional antiferromagnets". In: *Phys. Rev. B* 86 (24 Dec. 2012), p. 245132.

[23] Laura Messio, Claire Lhuillier, and Grégoire Misguich. "Time reversal symmetry breaking chiral spin liquids: Projective symmetry group approach of bosonic mean-field theories". In: *Phys. Rev. B* 87 (12 Mar. 2013), p. 125127.

[24] T. Hahn. "Cuba—a library for multidimensional numerical integration". In: *Computer Physics Communications* 168.2 (2005), pp. 78–95.

[25] Rok Žitko. "SNEG – Mathematica package for symbolic calculations with second-quantization-operator expressions". In: *Computer Physics Communications* 182.10 (2011), pp. 2259–2264.

Appendix A

Technical Details

A.1 Details of Fourier Transformation

After we selected the Ansatz, we can preform FT to simplify H_{MF}. Here we will write the details of Fourier transformation for Ansatz 1. The notation $k_\gamma = \mathbf{k} \cdot \mathbf{a}_\gamma$ will be used. Convention of the fourier transformation used is

$$b_{i\alpha} = \frac{1}{\sqrt{N}} \sum_{\mathbf{k}} e^{-i\mathbf{k}\mathbf{r_i}} b_{\mathbf{k}\alpha}. \tag{A.1}$$

A.1.1 Fourier Transformation of B fields

Here, we write the steps of simplifying B fields terms. We will use the only totally symmetric ansatz to lower the number of parameters. An additional $\frac{1}{2}$ appears because of double counting of pairs.

$$\sum_{<i,j>} \left[(B_{ij})^* \frac{1}{2} b^\dagger_{i\alpha} b_{j\alpha} + B_{ij} \frac{1}{2} b^\dagger_{j\alpha} b_{i\alpha} \right] \tag{A.2a}$$

$$= \frac{1}{2N} \sum_{i;\gamma,j=i\pm a_\gamma} \sum_{\mathbf{k},\mathbf{k'}} \left[(B_{ij})^* \frac{1}{2} b^\dagger_{\mathbf{k}\alpha} b_{\mathbf{k'}\alpha} e^{i(\mathbf{k}\mathbf{r_i} - \mathbf{k'}\mathbf{r_j})} + B_{ij} \frac{1}{2} b^\dagger_{\mathbf{k'}\alpha} b_{\mathbf{k}\alpha} e^{-i(\mathbf{k}\mathbf{r_i} - \mathbf{k'}\mathbf{r_j})} \right] \tag{A.2b}$$

$$= \frac{1}{2N} \sum_{i,\gamma} \sum_{\mathbf{k},\mathbf{k'}} \left[(B_{i(i\pm\gamma)})^* \frac{1}{2} b^\dagger_{\mathbf{k}\alpha} b_{\mathbf{k'}\alpha} e^{i(\mathbf{k}-\mathbf{k'})\mathbf{r_i} - i\pm\mathbf{k'}\mathbf{a}_\gamma} + B_{i(i\pm\gamma)} \frac{1}{2} b^\dagger_{\mathbf{k'}\alpha} b_{\mathbf{k}\alpha} e^{-i(\mathbf{k}\mathbf{r_i} - \mathbf{k'}\mathbf{r_j})} \right] \tag{A.2c}$$

$$= \frac{1}{4} \sum_{\mathbf{k}} \left[(B_{0(\pm\gamma)})^* b^\dagger_{\mathbf{k}\alpha} b_{\mathbf{k}\alpha} e^{\mp i\mathbf{k}\mathbf{a}_\gamma} + B_{0(\pm\gamma)} b^\dagger_{\mathbf{k}\alpha} b_{\mathbf{k}\alpha} e^{\pm i\mathbf{k}\mathbf{a}_\gamma} \right]. \tag{A.2d}$$

Writing $B = |B| e^{i\phi_B}$:

$$= \sum_{\mathbf{k}} \left[|B| \cos(k_\gamma + \phi_B) b^\dagger_{\mathbf{k}\alpha} \sigma^\gamma_{\alpha\beta} b_{\mathbf{k}\beta} \right]. \tag{A.3}$$

For later we can split the sum over $\mathbf{k}$ to sums over $\mathbf{k}$ and $-\mathbf{k}$ and we get an additional factor of 1/2.

A.1.2 Fourier Transformation of A fields

Here we need to be careful because $A_{ij} = -A_{ji}$.

$$\sum_{<i,j>} \left[(A_{ij})^* \frac{1}{2} \epsilon_{\alpha\beta} b_{i\alpha} b_{j\beta} + A_{ij} \frac{1}{2} (\epsilon_{\alpha\beta}) b^\dagger_{j\beta} b^\dagger_{i\alpha} \right] \tag{A.4a}$$

$$= \frac{1}{4N} \sum_{i,j=i\pm e_\gamma} \sum_{\mathbf{k},\mathbf{k'}} \left[(A_{ij})^* \epsilon_{\alpha\beta} b_{\mathbf{k}\alpha} b_{\mathbf{k'}\beta} e^{i(-\mathbf{k r_i} - \mathbf{k'} \mathbf{r_j})} + A_{ij} \epsilon_{\alpha\beta} b^\dagger_{\mathbf{k}\alpha} b^\dagger_{\mathbf{k'}\beta} e^{i(\mathbf{k r_i} + \mathbf{k'} \mathbf{r_j})} \right] \tag{A.4b}$$

$$= \frac{1}{4} \sum_{\mathbf{k},\gamma} \left[(A_{0\pm e_\gamma})^* \epsilon_{\alpha\beta} b_{\mathbf{k}\alpha} b_{-\mathbf{k}\beta} e^{i(\mathbf{k}(\pm \mathbf{a}_\gamma))} + A_{0\pm e_\gamma} \epsilon_{\alpha\beta} b^\dagger_{\mathbf{k}\alpha} b^\dagger_{-\mathbf{k}\beta} e^{-i\mathbf{k}(\pm \mathbf{a}_\gamma)} \right]. \tag{A.4c}$$

The form of the ansatz is now used to determine the directions of A fields. They are positive along a_γ directions.

$$= \frac{1}{4} \sum_{\mathbf{k},\gamma} \left[(A_{0e_\gamma})^* \epsilon_{\alpha\beta} b_{\mathbf{k}\alpha} b_{-\mathbf{k}\beta} (e^{i\mathbf{k}_\gamma} - e^{-i\mathbf{k}_\gamma}) + A_{0e_\gamma} \epsilon_{\alpha\beta} b^\dagger_{\mathbf{k}\alpha} b^\dagger_{-\mathbf{k}\beta} (e^{-i\mathbf{k}_\gamma} - e^{+i\mathbf{k}_\gamma}) \right] \tag{A.5a}$$

$$= \frac{1}{2} \sum_{\mathbf{k},\gamma} \left[(A_{0e_\gamma})^* \epsilon_{\alpha\beta} b_{\mathbf{k}\alpha} b_{-\mathbf{k}\beta} i \sin k_\gamma + A_{0e_\gamma} \epsilon_{\alpha\beta} b^\dagger_{\mathbf{k}\alpha} b^\dagger_{-\mathbf{k}\beta} (-i \sin k_\gamma) \right]. \tag{A.5b}$$

In the case of the totally symmetric ansatz the A fields are real and we are left with:

$$\frac{i}{2} A (\sin k_1 + \sin k_2 + \sin k_3) \sum_{\mathbf{k}} \left[(b_{\mathbf{k}\uparrow} b_{-\mathbf{k}\downarrow} - b_{\mathbf{k}\downarrow} b_{-\mathbf{k}\uparrow}) - (b^\dagger_{\mathbf{k}\uparrow} b^\dagger_{-\mathbf{k}\downarrow} - b^\dagger_{\mathbf{k}\downarrow} b^\dagger_{-\mathbf{k}\uparrow}) \right]. \tag{A.5c}$$

A.1.3 Fourier Transformation of t fields

The situation is identical to the case of A fields, the only difference is that bonds do not have a direction since $t_{ij} = t_{ji}$. For the totally symmetric ansatz, t fields are also real.

$$\sum_{<i,j>} \left[(t^\gamma_{ij})^* \hat{t}^\gamma_{ij} + t^\gamma_{ij} (\hat{t}^\gamma_{ij})^\dagger \right] = \frac{1}{2} t \sum_{\mathbf{k},\gamma} (\hat{t}^\gamma_{\mathbf{k}} + (\hat{t}^\gamma_{\mathbf{k}})^\dagger) \cos k_\gamma, \tag{A.6}$$

where operator $\hat{t}^\gamma_{\mathbf{k}}$ is operator $\hat{t}^\gamma_{ij}$ with the substitution

$$b_{i\alpha} \to b_{\mathbf{k}\alpha}, \qquad\qquad b_{j\alpha} \to b_{\mathbf{k}\alpha}. \tag{A.7}$$

A.2 Static Spin Structure Factor

We have derived that the spin structure factor has elements of the form:

$$S^{cd}(\mathbf{q}) = \frac{1}{\mathrm{Vol}_k} \int \mathrm{d}^2 k f^{cd}(P_{\mathbf{k}}, P_{\mathbf{k+q}}). \tag{A.8}$$

Here we will only show $f^{xx}(P_{\mathbf{k}}, P_{\mathbf{k+q}})$:

$$
\begin{aligned}
f^{xx}(P_{\mathbf{k}}, P_{\mathbf{k+q}}) = \frac{1}{4}\big(&P_{\mathbf{k}23}P_{\mathbf{k+q}21}P^*_{\mathbf{k}13}P^*_{\mathbf{k+q}11} + P_{\mathbf{k}13}P_{\mathbf{k+q}11}P^*_{\mathbf{k}23}P^*_{\mathbf{k+q}21} \\
&+ P_{\mathbf{k}23}P_{\mathbf{k+q}22}P^*_{\mathbf{k}13}P^*_{\mathbf{k+q}12} + P_{\mathbf{k}13}P_{\mathbf{k+q}12}P^*_{\mathbf{k}23}P^*_{\mathbf{k+q}22} + P_{\mathbf{k}33}P_{\mathbf{k+q}21}P^*_{\mathbf{k}13}P^*_{\mathbf{k+q}41} \\
&+ P_{\mathbf{k}33}P_{\mathbf{k+q}22}P^*_{\mathbf{k}13}P^*_{\mathbf{k+q}42} + P_{\mathbf{k}43}P_{\mathbf{k+q}21}P^*_{\mathbf{k}13}P^*_{\mathbf{k+q}31} + P_{\mathbf{k}43}P_{\mathbf{k+q}22}P^*_{\mathbf{k}13}P^*_{\mathbf{k+q}32} \\
&+ P_{\mathbf{k}13}P_{\mathbf{k+q}21}P^*_{\mathbf{k}13}P^*_{\mathbf{k+q}21} + P_{\mathbf{k}13}P_{\mathbf{k+q}22}P^*_{\mathbf{k}13}P^*_{\mathbf{k+q}22} + P_{\mathbf{k}24}P_{\mathbf{k+q}21}P^*_{\mathbf{k}14}P^*_{\mathbf{k+q}11} \\
&+ P_{\mathbf{k}14}P_{\mathbf{k+q}11}P^*_{\mathbf{k}24}P^*_{\mathbf{k+q}21} + P_{\mathbf{k}24}P_{\mathbf{k+q}22}P^*_{\mathbf{k}14}P^*_{\mathbf{k+q}12} + P_{\mathbf{k}14}P_{\mathbf{k+q}12}P^*_{\mathbf{k}24}P^*_{\mathbf{k+q}22} \\
&+ P_{\mathbf{k}34}P_{\mathbf{k+q}21}P^*_{\mathbf{k}14}P^*_{\mathbf{k+q}41} + P_{\mathbf{k}34}P_{\mathbf{k+q}22}P^*_{\mathbf{k}14}P^*_{\mathbf{k+q}42} + P_{\mathbf{k}44}P_{\mathbf{k+q}21}P^*_{\mathbf{k}14}P^*_{\mathbf{k+q}31} \\
&+ P_{\mathbf{k}44}P_{\mathbf{k+q}22}P^*_{\mathbf{k}14}P^*_{\mathbf{k+q}32} + P_{\mathbf{k}14}P_{\mathbf{k+q}21}P^*_{\mathbf{k}14}P^*_{\mathbf{k+q}21} + P_{\mathbf{k}14}P_{\mathbf{k+q}22}P^*_{\mathbf{k}14}P^*_{\mathbf{k+q}22} \\
&+ P_{\mathbf{k}33}P_{\mathbf{k+q}11}P^*_{\mathbf{k}23}P^*_{\mathbf{k+q}41} + P_{\mathbf{k}33}P_{\mathbf{k+q}12}P^*_{\mathbf{k}23}P^*_{\mathbf{k+q}42} + P_{\mathbf{k}43}P_{\mathbf{k+q}11}P^*_{\mathbf{k}23}P^*_{\mathbf{k+q}31} \\
&+ P_{\mathbf{k}43}P_{\mathbf{k+q}12}P^*_{\mathbf{k}23}P^*_{\mathbf{k+q}32} + P_{\mathbf{k}23}P_{\mathbf{k+q}11}P^*_{\mathbf{k}23}P^*_{\mathbf{k+q}11} + P_{\mathbf{k}23}P_{\mathbf{k+q}12}P^*_{\mathbf{k}23}P^*_{\mathbf{k+q}12} \\
&+ P_{\mathbf{k}34}P_{\mathbf{k+q}11}P^*_{\mathbf{k}24}P^*_{\mathbf{k+q}41} + P_{\mathbf{k}34}P_{\mathbf{k+q}12}P^*_{\mathbf{k}24}P^*_{\mathbf{k+q}42} + P_{\mathbf{k}44}P_{\mathbf{k+q}11}P^*_{\mathbf{k}24}P^*_{\mathbf{k+q}31} \\
&+ P_{\mathbf{k}44}P_{\mathbf{k+q}12}P^*_{\mathbf{k}24}P^*_{\mathbf{k+q}32} + P_{\mathbf{k}24}P_{\mathbf{k+q}11}P^*_{\mathbf{k}24}P^*_{\mathbf{k+q}11} + P_{\mathbf{k}24}P_{\mathbf{k+q}12}P^*_{\mathbf{k}24}P^*_{\mathbf{k+q}12}\big).
\end{aligned}
\tag{A.9}
$$

Declaration of Authorship

I hereby certify that this master thesis has been composed by myself, and describes my own work, unless otherwise acknowledged in the text. All references have been quoted, and all sources of information have been specifically acknowledged. It has not been accepted in any previous application for a degree.

Location, date	Signature